

Safe MPC Alignment with Human Directional Feedback

Zhixian Xie, Wenlong Zhang, Yi Ren, Zhaoran Wang, George J. Pappas, Wanxin Jin

Abstract—In safety-critical robot planning or control, manually specifying safety constraints or learning them from demonstrations can be challenging. In this paper, we propose a certifiable alignment method for a robot to learn a safety constraint in its model predictive control (MPC) policy with human online directional feedback. To our knowledge, it is the first method to learn safety constraints from human feedback. The proposed method is based on an empirical observation: human directional feedback, when available, tends to guide the robot toward safer regions. The method only requires the direction of human feedback to update the learning hypothesis space. It is certifiable, providing an upper bound on the total number of human feedback in the case of successful learning of safety constraints, or declaring the misspecification of the hypothesis space, i.e., the true implicit safety constraint cannot be found within the specified hypothesis space. We evaluated the proposed method using numerical examples and user studies in two developed simulation games. Additionally, we implemented and tested the proposed method on a real-world Franka robot arm performing mobile water-pouring tasks in a user study. The simulation and experimental results demonstrate the efficacy and efficiency of our method, showing that it enables a robot to successfully learn safety constraints with a small handful (tens) of human directional corrections.

Index Terms—Learning from Human Feedback, Constraint Inference, Model Predictive Control, Human-Robot Interaction, Cutting-Plane Method.

I. INTRODUCTION

In developing robot control policies, ensuring safety is always the top priority. This is especially crucial for safety-critical applications, such as autonomous vehicles or collaborative robots operating near human users, where violating safety constraints can lead to irreversible loss or damage.

While a significant line of work in safe control [1] and safe reinforcement learning [2] focuses on the safe policy design given robot behavior constraints, less attention has been paid to how to specify the safety constraints in the first place. In fact,

Zhixian Xie and Wanxin Jin are with the Intelligent Robotics and Interactive Systems (IRIS) Lab in the School for Engineering of Matter, Transport and Energy at Arizona State University. Wanxin Jin is the corresponding author. Emails: zxxie@asu.edu and wanxinjin@gmail.com.

Wenlong Zhang is with the Polytechnic School at Arizona State University. Email: wenlong.zhang@asu.edu.

Yi Ren is with the School for Engineering of Matter, Transport and Energy at Arizona State University. Email: yiren@asu.edu.

Zhaoran Wang is with the Departments of Industrial Engineering & Management Sciences, Northwestern University. Email: zhaoranwang@gmail.com.

George J. Pappas is with the Department of Electrical and Systems Engineering at the University of Pennsylvania. Email: pappasg@seas.upenn.edu.

This work involved human subjects or animals in its research. Approval of all ethical and experimental procedures and protocols was granted by ASU's Institutional Review Board under Application No. STUDY00020060, and performed in the line with Title 45 of the Code of Federal Regulations, Part 46 (45 CFR 46).

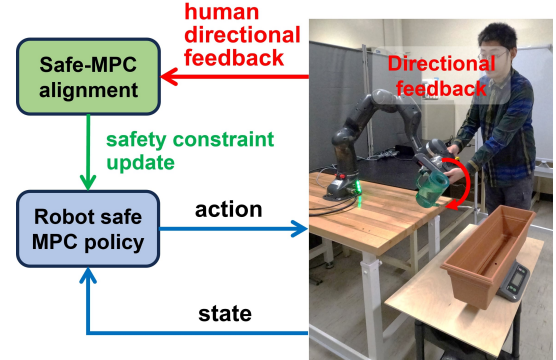


Fig. 1. Overall illustration of the proposed method. The proposed safe MPC alignment online updates the safety constraint in the robot safe MPC policy with human directional feedback, such that the robot eventually aligns the safe MPC policy with human intent for accomplishing safety-critical tasks.

for many daily tasks and applications, specifying proper safety constraints can be challenging due to two main reasons. First, *explicit safety boundary for robot behavior can be hard to model or define*. For example, in the task of a household robot feeding an elderly person, the complex nature of the task makes it very difficult to define a precise constraint for safe feeding behavior. Second, *safety specifications can vary among users and require personalization*. An example is lane-switching of an autonomous vehicle: aggressive drivers may prefer frequent lane-switching behavior, while conservative users may consider frequent lane-switching unsafe.

The challenges in safety specifications lead to two key questions, which we seek to answer in this paper. Q1: can a robot learn and align its safety constraints with human intent in an *intuitive and online* manner? Q2: can such learning process to be *user-data efficient* such that a robot is able to quickly adapt to different users?

Recent work [3]–[5] has proposed learning safety constraints from human demonstrations. However, these approaches face limitations that prevent them from fully addressing the two key questions. First, obtaining valid user demonstrations can be costly and time-consuming, especially with high-dimensional robot systems. Second, demonstration-based learning typically follows an offline or episodic learning procedure, which does not allow for on-the-fly interaction where human feedback and robot updates occur in real time.

This paper aims to answer the previous two questions by proposing a new paradigm for a robot to online and efficiently learn safety constraints in its model predictive control (MPC) policy with human feedback. We name the

method *safe MPC alignment*. As shown in Fig. 1, a human user, while observing the robot’s potentially unsafe behavior, provides directional feedback for the robot’s motion. Once receiving the human feedback, the robot immediately updates the safety constraints in its MPC policy and continues its motion with the updated policy. Human feedback is in the form of physical corrections [6], [7] and sparse in time. The *safe MPC alignment* only utilizes the direction of human correction, regardless of the magnitude, for the safety constraints update. Importantly, the procedure of the proposed alignment is able to guarantee the exponential convergence with finite rounds of human corrections, or output failure with identified hypothesis misspecification. Specifically, we highlight our main contributions below.

(I) We propose the method of *safe MPC alignment* with human directional feedback. The method enables a robot to online learn a safe MPC policy from human directional corrections. To our knowledge, it is the first work for interactive learning of safety constraints from human feedback.

(II) We theoretically show the human-data efficiency of the proposed *safe MPC alignment* method: the proposed method is guaranteed to have exponential convergence with finite human interactions/corrections. Furthermore, we also prove that the proposed algorithm enables the identification of hypothesis space misspecification failure.

(III) We conduct extensive user studies to validate the effectiveness of the proposed method, including user studies on two MuJoCo-based simulation games and one real-world experiment of physically teaching a Franka robot arm for mobile liquid pouring. The results demonstrate the effectiveness and efficiency of the proposed method and show that a robot can successfully learn a safe MPC policy with only tens of human corrections.

The remaining paper is organized as follows. Section II reviews the related work, and Section III formulates the safe MPC alignment problem. The main algorithm is presented in Section IV. Section V focuses on the implementation details of the algorithm and presents the main results on convergence and misspecification. Sections VI and VII provide the results of numerical experiments and user studies. Conclusions are drawn in Section VIII.

II. RELATED WORK

A. Learning from Demonstrations

Under the general theme of learning from human data, the proposed work is loosely connected to the topic of learning from demonstrations, where objective functions are learned from expert (human) data using techniques of inverse reinforcement learning (IRL) and inverse optimal control (IOC) [8], [9]. Since the demonstration data typically comes as time sequences of data, IRL/IOC methods typically run in an offline or episodic manner: a robot first obtains human demonstrated trajectories, and then performs reward/cost learning [9]–[14]. As pointed in [15], acquiring optimal demonstration data can be difficult in practice. The challenge can be either attributed to higher degrees of freedom of the robot, or the lack of prior knowledge about the desired robot behavior [16].

In this work, we focus on online and interactive learning of safety constraints. Different from learning from demonstrations that needs the exhibition of desired robot behavior, the proposed learning paradigm only requires a human user to incrementally improve the current robot motion by providing directional feedback, thus more accessible to human users.

B. Learning from Human Interaction

Orthogonal to learning from demonstrations is robot learning from human interaction. The line of this work typically focus on learning a reward/cost function from human feedback, which can be in the form of preference and corrections/feedback. The learned reward/cost function is then used to derive human-preferred robot policy. In learning from human preferences, human preference typically given as user’s ranking of two or multiple robot candidate trajectories [17]–[23], and Bradley-Terry model [24] is used to update the reward/cost function. The recently variant in this line of work seeks to directly learn a policy from human preference [25].

Human interaction can also come as corrections, where human users may intervene and correct the robot at runtime. An intended robot reward/cost function can be inferred from human corrections. Specific human corrections include language [26]–[30] and physical corrections in trajectory/action space [6], [31], [32]. Since human corrections can be sparse in time, many methods [6], [31]–[36] use trajectory deformation to convert sparse corrections to a continuous human-intended trajectory using a temporal propagation kernel. The reward/cost function is updated to explain the deformed trajectories. Some strategies are further proposed to deal with the uncertainty and improve the robustness of the learning process, like updating one parameter dimension at a time [32] or formulating the reward/cost learning in the framework of Kalman Filter [33].

Our work also belongs to the category of learning from human physical corrections. But instead of learning reward/cost functions, we focus on learning safety constraints from human corrections, which has not been addressed before. Methodologically, we propose a certifiable learning method, which guarantees the exponential learning convergence with few human corrections or identifies the hypothesis misspecification when the learning hypothesis space does not contain the true human intent. Those capabilities are missing in existing methods. For example, the state-of-the-art methods [37] for learning from human preference requires hundreds or thousands of human feedback, while the proposed method can successfully learn a complex safe policy only with tens of human corrections.

C. Learning Constraints from Demonstrations

A increasing number of work focuses on learning safety constraints from demonstrations. One vanilla idea is to formulate constraint learning as a binary classification. However, different from learning reward/cost, since a robot usually runs within a safe region, negative demonstration samples that violate safety constraints are challenge to collect. To collect negative samples, different strategies have been proposed. [3], [38] consider the trajectories of lower cost as the unsafe samples. [39] proposes adjusting the constraints toward decreasing the safety margin

of feasible policies. Safety constraints can also be learned via mixed integer programming [3], [38], pessimistic adjustment [39], and no-regret algorithm [40].

Another line of work attempts to learn safety constraints only from safe demonstration data. For example, some work exploits the optimality of demonstration with unknown constraints [41]–[43]. Different probabilistic formulations are also proposed to learn constraints from demonstration data, such as maximum likelihood [5], [44], [45], maximum causal entropy [46], [47], and Bayesian inference [48], [49]. In the constraint learning, safety constraints can be represented as a set of safe states [41], the belief of potential constraints [42], Gaussian process [43], or directly as a convex hull in policy space [4].

The vast majority of existing approaches focus on learning safety constraints from human demonstrations. They are mostly developed in the setting of reinforcement learning, needing to repetitively solve policy optimization in each learning update. Those methods cannot be used in an online, interactive setting, where a robot is expected to immediately update its safe policy and respond to feedback given by a human user. To achieve so, we will develop the first method, to our best knowledge, to enable learning the safe constraint from human feedback.

III. PRELIMINARY AND PROBLEM FORMULATION

A. Safe Model Predictive Control

We consider the following safe model predictive control (Safe MPC) for a robotic system, where the safety constraint is learnable and parameterized by $\theta \in \mathbb{R}^r$.

$$\begin{aligned} \min_{\mathbf{u}_{0:T-1}} \quad & J(\mathbf{u}_{0:T-1}; \mathbf{x}_0) = \sum_{t=0}^{T-1} c(\mathbf{x}_t, \mathbf{u}_t) + h(\mathbf{x}_T) \\ \text{subject to} \quad & \mathbf{x}_{t+1} = \mathbf{f}(\mathbf{x}_t, \mathbf{u}_t) \\ & g_\theta(\mathbf{x}_{0:T}, \mathbf{u}_{0:T-1}) \leq 0 \end{aligned} \quad (1)$$

Here, $\mathbf{x}_t \in \mathbb{R}^n$ and $\mathbf{u}_t \in \mathbb{R}^m$ are robot state and action, respectively, at time step $t = 0, 1, 2, \dots, T$ with T being the prediction horizon; $\mathbf{x}_{0:T} = (\mathbf{x}_0, \mathbf{x}_1, \dots, \mathbf{x}_T)$ and $\mathbf{u}_{0:T-1} = (\mathbf{u}_0, \mathbf{u}_1, \dots, \mathbf{u}_{T-1})$; $J(\cdot)$ is the given cost function including the running cost term $c(\cdot)$ and final cost term $h(\cdot)$, representing the given task; $\mathbf{f}(\cdot, \cdot)$ is the system dynamics; $g_\theta(\cdot)$ is the safety constraint, which is parameterized by θ . Given starting state \mathbf{x}_0 and constraint parameter θ , the trajectory solution to (1), denoted as $\xi_\theta = \{\mathbf{u}_{0:T-1}^\theta, \mathbf{x}_{0:T}^\theta\}$, is an implicit function of θ .

In a receding horizon implementation, \mathbf{x}_0 is set as the robot's current state (estimation) \mathbf{x}_k , where $k = 0, 1, 2, \dots$, is the policy rollout time step; and only the first action \mathbf{u}_0^θ in $\mathbf{u}_{0:T}^\theta$ is applied to the robot to move the robot to the next state \mathbf{x}_{k+1} . This leads to a closed-loop Safe MPC policy for the robotic system, denoted as π_θ , mapping from robot current state \mathbf{x}_k to its action \mathbf{u}_0^θ .

B. Safe Asymptotic Approximation of Safe MPC

We present a penalty-based approximation to the original Safe MPC problem (1). Define variable $\xi = \{\mathbf{u}_{0:T-1}, \mathbf{x}_{0:T}\}$ and a penalty objective for (1) that incorporates the cost $J(\xi)$ and safety constraint $g_\theta(\xi)$:

$$B(\xi, \theta) = J(\xi) - \gamma \ln(-g_\theta(\xi)). \quad (2)$$

We have the following result from our prior work [50], stating an asymptotic and safe approximation to the solution ξ_θ to (1) by the following optimization

$$\min_{\mathbf{u}_{0:T-1}} B(\xi, \theta) \quad \text{subject to} \quad \mathbf{x}_{t+1} = \mathbf{f}(\mathbf{x}_t, \mathbf{u}_t). \quad (3)$$

Lemma 1. (Theorem 2 in [50]) *If the original Safe MPC problem (1) satisfies certain mild conditions (i.e., local second-order condition and strict complementarity), then for any small $\gamma > 0$, there exists a (local) solution $\xi_\theta^\gamma = \{\mathbf{u}_{0:T-1}^{\theta, \gamma}, \mathbf{x}_{0:T}^{\theta, \gamma}\}$ to (3), and ξ_θ^γ is safe with respect to the original constraint, i.e., $g_\theta(\xi_\theta^\gamma) < 0$. Furthermore, ξ_θ^γ is asymptotically approximate the original solution to (1): $\xi_\theta^\gamma \rightarrow \xi_\theta$ as $\gamma \rightarrow 0$.*

The above lemma asserts that by solving (3) one can safely use the approximate solution ξ_θ^γ to replace the original solution with arbitrary controlled accuracy by γ . As shown in [50], γ usually takes a small value for good approximation accuracy. In the development below, we fix the parameter γ in (3). We denote the approximate Safe MPC in (3) as π_θ^γ .

C. Problem Formulation

1) *Representation of Human Intended Safety:* We consider the scenario of human-robot coexistence, where a human is supervising the robot for a given task. The user has his/her intent of robot safety. In Safe MPC (1), we hypothesize that the user intended safety can be represented by the set

$$\mathcal{S}(\theta_H) = \{(\mathbf{x}_{0:T}, \mathbf{u}_{0:T-1}) \mid g_{\theta_H}(\mathbf{x}_{0:T}, \mathbf{u}_{0:T-1}) \leq 0\}. \quad (4)$$

Here, θ_H is user implicit intent parameter picked from an implicit set $\Theta_H \subset \mathbb{R}^r$, i.e., $\theta_H \in \Theta_H$. Θ_H is implicit to the human user and unknown to the robot. For the robot policy π_θ^γ , if $\theta \in \Theta_H$, the user considers the robot behavior to be safe; otherwise if $\theta \notin \Theta_H$, the robot motion by π_θ^γ might not be safe at certain time in the view of the user, and thus the user provides corrections to improve the safety of the robot.

We use an implicit set $\Theta_H \in \mathbb{R}^r$, instead of single point θ_H , to capture the potential variation of user intents. We suppose that a volume measure of Θ_H , $\text{Vol}(\Theta_H)$, is non-zero, and a user intent $\theta_H \in \Theta_H$ can vary at different steps and context, but always within Θ_H .

2) *Human Online Directional Correction:* We consider a human user who gives correction to the robot in an online fashion while the robot is running with the most updated π_θ^γ . Specifically, denote i to be the index of learning update, and suppose the robot policy currently is $\pi_{\theta_i}^\gamma$. At the time steps k_i of rolling out $\pi_{\theta_i}^\gamma$, a human user gives directional correction \mathbf{a}_{k_i} in robot action space at its state \mathbf{x}_{k_i} . After receiving \mathbf{a}_{k_i} , the robot updates the safety parameter $\theta_i \rightarrow \theta_{i+1}$ in (1) and obtain the updated policy $\pi_{\theta_{i+1}}^\gamma$. Then, the robot continues with the updated policy $\pi_{\theta_{i+1}}^\gamma$ until the next user possible correction. This process of robot MPC policy update and user correction repeats until the convergence of the policy update or the user is satisfied with the robot motion. An illustration of one update is shown in Fig. 2.

In the above-stated human feedback process, we consider that a human user only provides directional correction \mathbf{a} , i.e., the magnitude $\|\mathbf{a}\|$ does not matter (theoretical justification

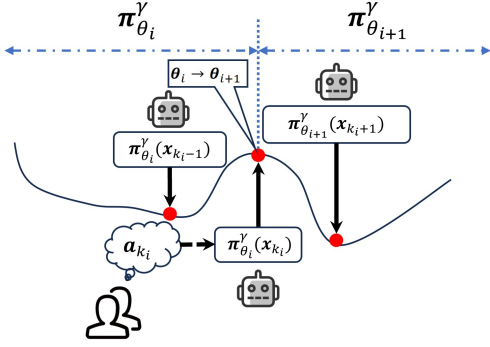


Fig. 2. Update of safe MPC policy with human directional corrections.

will be given later in Section IV-A). For example, when correcting a mobile robot, the user's correction can be "left" or "right", without specifying how much the robot should go. Also, we assume that the user feedback is applied in the action space. For some robotic systems, this assumption can be readily met, such as turning the driving wheels for autonomous vehicles. In other cases, the correction can be applied through a dedicated (hardware or algorithmic) interface to the action space; such as contact forces from end-effector to joint torque, and teleoperation device for remote control. In those cases, \mathbf{a} is the correction signal after the interface. The reason why we only consider the correction in action space is that otherwise the corrections in robot state space can lead to dynamics unfeasibility or uncontrollability for under-actuated robotic systems [7], [51].

3) *Robot Operation Safety and Emergency Stop*: In the aforementioned policy update procedure, the robot will respond to human corrections by executing the updated safe MPC policy π_θ . However, it is possible that the robot may still exit the user-intended safety zone during the correction process. In such cases, a human user may trigger an emergency stop to stop the robot motion and potentially restart it from a desired safety region. This emergency stop mechanism is common in real-world robotic applications. Until an emergency stop is triggered, human corrections typically occur while the robot is still within the intended safety zone; otherwise, the corrections would be useless. For instance, correcting an autonomous vehicle after it has been crashed is futile.

4) *Parametric Safety Constraints*: In the safe MPC (1), the safety set is defined as a zero sublevel set of a safety value function g_θ . We note that if g_θ has sufficient representation power, the safety set can represent complex safety region, which can be alternatively represented by the intersection of multiple constraints (e.g., a polytope safety set defined by multiple hyperplanes). In the following, we mainly focus on a weighted-features parameterization of g_θ , which has been commonly used by the extensive prior work on learning cost/reward [4], [7], [52]–[54]. Specifically, we parameterize g_θ

$$g_\theta(\mathbf{x}_{0:T}, \mathbf{u}_{0:T-1}) = \phi_0(\mathbf{x}_{0:T}, \mathbf{u}_{0:T-1}) + \theta_1 \phi_1(\mathbf{x}_{0:T}, \mathbf{u}_{0:T-1}) + \theta_2 \phi_2(\mathbf{x}_{0:T}, \mathbf{u}_{0:T-1}) + \dots + \theta_r \phi_r(\mathbf{x}_{0:T}, \mathbf{u}_{0:T-1}), \quad (5)$$

with $\theta = [\theta_1, \theta_2, \dots, \theta_r]^T \in \mathbb{R}^r$ and $\phi = [\phi_1, \phi_2, \dots, \phi_r]^T$ the weight and feature vectors, respectively. We fix the weight of

ϕ_0 as unit, because otherwise, the θ is scaling ambiguous, i.e., any scaled $c \cdot \theta$ with $c > 0$ lead to the same MPC solutions. We do not impose any constraints on the choice of feature vector as long as it is differentiable. For example, ϕ can be neural features. Later, we will discuss our proposed method for generic parameterization g_θ .

5) *Problem of Safe MPC Alignment*: Following the procedure of online human correction and robot policy update described in Subsection III-C and given a weighted-feature safety constraint (5), the interest of this work is to develop a policy update rule: $\theta_i \rightarrow \theta_{i+1}$ with each human directional correction, such that $\theta_i \rightarrow \theta_H \in \Theta_H$, as $i = 1, 2, 3, \dots$, i.e., the safety constraint in the robot safe MPC policy will be aligned with human intent.

IV. ALGORITHM OVERVIEW FOR SAFE MPC ALIGNMENT

A. Hypothesis on User Directional Feedback

In this session, we will introduce a hypothesis on user directional correction, which lays the foundation for our alignment framework proposed subsequently. Informally, we have the following intuitions on user feedback. First, user directional corrections, on average, improve the robot safety. The similar assumption is the basis for reinforcement learning with human feedback [55]. Second, user correction on robot safety is typically proactive and typically happens before the robot enters into the true unsafe region. In other words, human correction is made when the robot operates within $\mathcal{S}(\theta_H)$ in (4). For example, it is useless to correct a ground vehicle after its collision with obstacles. Third, with the second intuition, user feedback is typically safety-margin aware: the closer a robot gets to the boundary of the unsafe region, the more significant user safety correction will be. This is observed in our prior user study [7]. In the following, we will formalize those intuitions.

Suppose that robot motion plan ξ_θ^γ is solved from (3) with parameter θ , and a human user applies directional correction \mathbf{a} at first time step 0. Define

$$\mathbf{a} = (\mathbf{a}^T, 0, 0, \dots) \in \mathbb{R}^{mT}. \quad (6)$$

Formally, we assume there is a nonzero-volume set $\bar{\Theta}_H$ (containing a ball) in user implicit intent set Θ_H , i.e., $\bar{\Theta}_H \subseteq \Theta_H$, such that for any $\theta_H \in \bar{\Theta}_H$, the user directional correction \mathbf{a} , on average, indicates a direction of lowering the penalty value $B(\xi_\theta^\gamma, \theta_H)$ for the robot motion plan ξ_θ^γ . Concretely, it means \mathbf{a} on averages points in a direction of the negative gradient of $B(\xi, \theta_H)$ evaluated at ξ_θ^γ , i.e.,

$$\forall \theta_H \in \bar{\Theta}_H, \mathbb{E}_{\mathbf{a}} \langle \mathbf{a}, -\nabla B(\xi_\theta^\gamma, \theta_H) \rangle = \langle \bar{\mathbf{a}}, -\nabla B(\xi_\theta^\gamma, \theta_H) \rangle \geq 0. \quad (7)$$

Here, $\mathbb{E}_{\mathbf{a}}(\mathbf{a}) = \bar{\mathbf{a}}$ and the equality is due to the second term $\nabla B(\xi, \theta)$ is not dependent on \mathbf{a} . $\nabla B(\xi, \theta)$ denotes the full gradient of B with respect to $\mathbf{u}_{0:T-1}$ evaluated at trajectory $\xi = \{\mathbf{u}_{0:T-1}, \mathbf{x}_{0:T}\}$. Similar notations apply to J and g below. Since state sequence $\mathbf{x}_{0:T}$ is the rollout of $\mathbf{u}_{0:T-1}$ on dynamics, the differentiation goes through the dynamics equation.

One of the important observations to (7) is that the magnitude of the user correction \mathbf{a} does not affect the inequality. This

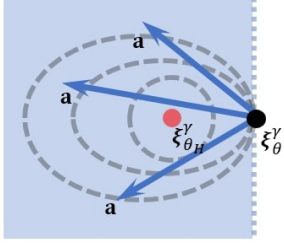


Fig. 3. Illustration of directional corrections in the space of robot motion plan ξ_s . The grey circles represent the level contours of $B(\xi, \theta_H)$. The black dot stands for current motion plan ξ_θ^γ and the red point stands for the plan $\xi_{\theta_H}^\gamma$ with human intended safety. The blue region stands for the half-space of all possible human corrections under our assumption. Some samples of human corrections are shown by blue arrows.

brings one advantage of directional correction compared to the magnitude-based correction: regardless of robot safeMPC plan ξ_θ^γ , the user directional correction always accounts for half of the action space, as shown in Figure 3. Extending (7) leads to

$$\forall \theta_H \in \bar{\Theta}_H, \langle \bar{\mathbf{a}}, -\nabla J(\xi_\theta^\gamma) \rangle + \gamma \frac{1}{-g_{\theta_H}(\xi_\theta^\gamma)} \langle \bar{\mathbf{a}}, -\nabla g_{\theta_H}(\xi_\theta^\gamma) \rangle \geq 0. \quad (8)$$

For the above equation, we have the following interpretations.

(I) The first and second terms on the left side of (8) correspond to the user's correction toward lowering the cost and improving the safety value of robot plan ξ_θ^γ . γ serves as a weight between two improvements.

(II) If we interpret the value of $-g_{\theta_H}(\xi_\theta^\gamma)$ as the safety margin of robot plan ξ_θ^γ , (8) indicates that user's correction is safety-margin aware: the closer the robot motion get to the unsafe region, the more significant a human user correction will be to drive the system back to safety interior. This property is consistent with our previous intuition.

(III) The above hypothesis (7) requires that $B(\xi_\theta^\gamma, \theta_H)$ is well-defined in the first place, i.e.,

$$\forall \theta_H \in \bar{\Theta}_H, \quad g_{\theta_H}(\xi_\theta^\gamma) < 0. \quad (9)$$

The requirement corresponds to the third intuition — a user typically makes correction only when the robot is within user intended safety region, i.e., $\xi_\theta^\gamma \in \mathcal{S}(\theta_H)$.

In sum, we have used (7) and (9) to formalize the intuitions we have observed at the beginning of this session. Those two constraints on θ_H will be used in the robot learning pipeline developed in the next session.

B. Alignment Algorithm: Learning by Hypothesis Space Cutting

To find an implicit $\theta_H \in \bar{\Theta}_H \subseteq \Theta$ for the safe MPC (1), our idea is that at any learning iteration $i = 0, 1, 2, \dots$, the robot monitors and updates a hypothesis space $\Theta_i \in \mathbb{R}^r$, a set containing all possible $\bar{\Theta}_H$. At initial, the robot may choose a hypothesis space Θ_0 that is large enough to contain $\bar{\Theta}_H$. Specifically, one can choose

$$\Theta_0 = \{\theta \mid c_l \leq \theta \leq c_h\} \subset \mathbb{R}^r, \quad (10)$$

in which c_l, c_h are the given bounding vectors. By specifying a Θ_0 large enough, we assume

$$\bar{\Theta}_H \subset \Theta_0. \quad (11)$$

Later, we will that our alignment algorithm can self-access the failure of learning in case of misspecification, where (11) is not met.

Recall the procedure of human correction in Section III-C and Fig. 2. At i -th learning update, $i = 1, 2, 3, \dots$, the robot safe MPC policy $\pi_{\theta_i}^\gamma$ with $\theta_i \in \Theta_{i-1}$. The user gives a directional correction \mathbf{a}_{k_i} at rollout step k_i . By letting $\bar{\mathbf{a}}_i = (\mathbf{a}_{k_i}^T, 0, 0, \dots)$ as in (6), we can establish the following two constraints on $\bar{\Theta}_H$ from the previous hypothesis (7) and (9)

$$\bar{\Theta}_H \subset \mathcal{C}_i = \{\theta \mid \langle \bar{\mathbf{a}}_i, \nabla B(\xi_{\theta_i}^\gamma, \theta) \rangle \leq 0, \quad g_{\theta}(\xi_{\theta_i}^\gamma) < 0\}, \quad (12)$$

which we refer to as the *cutting set*. Using \mathcal{C}_i , one can update the hypothesis space

$$\Theta_i = \Theta_{i-1} \cap \mathcal{C}_i. \quad (13)$$

The above update can be viewed as a step of using the cutting set (12) to cut the current hypothesis space Θ_{i-1} to remove the portion where $\bar{\Theta}_H$ is impossible. The remaining hypothesis space Θ_i will be new hypothesis used in the next iteration. With the above update, we have the following result.

Lemma 2. *Given $\bar{\Theta}_H \subset \Theta_0$, if one follows the update (13), then $\bar{\Theta}_H \subset \Theta_i$ for all $i = 1, 2, 3, \dots$*

Proof. See the proof in Appendix A-A. \square

As shown by Fig. 4, the procedure of robot learning is to cut and move hypothesis space based on human directional correction. Therefore, we name our alignment method *Hypothesis Space Cutting*. As a summary, we present the three main steps of the hypothesis space cutting updates below.

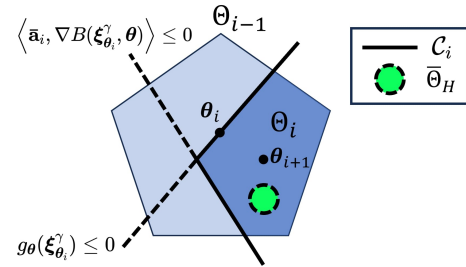


Fig. 4. The update of constraint parameter (2D examples). Two cutting lines are used to cut Θ_{i-1} to Θ_i . The user implicit intent set $\bar{\Theta}_H$ is contained in Θ_i . New θ_{i+1} is chosen as the parameter for the next safe MPC policy.

Safe MPC alignment by Hypothesis Space Cutting

Initialize Θ_0 that contains $\bar{\Theta}_H$. Repeat the following three steps for $i = 1, 2, \dots, K$ until $\theta_i \in \bar{\Theta}_H$.

Step 1: Robot chooses parameter $\theta_i \in \Theta_{i-1}$ for its current safe MPC policy $\pi_{\theta_i}^\gamma$.

Step 2: Human user applies a directional correction \mathbf{a}_{k_i} while robot executes $\pi_{\theta_i}^\gamma$.

Step 3: Perform hypothesis space cut using (13) to get new hypothesis space Θ_i .

At i th iteration of the Hypothesis Space Cutting, the robot chooses $\theta_i \in \Theta_{i-1}$ from the most recent hypothesis space Θ_{i-1} for its current safe MPC $\pi_{\theta_i}^\gamma$. While executing $\pi_{\theta_i}^\gamma$, the robot receives human directional correction \mathbf{a}_{k_i} at the rollout time step k_i . This correction is used to induce the cutting set \mathcal{C}_i (12), which will be used to update Θ_{i-1} to Θ_i in (13). The above iteration repeats $i = 1, 2, 3, \dots$

From (13) and by following the above hypothesis space cutting method, one can easily see that $\Theta_0 \supseteq \Theta_1 \supseteq \Theta_2 \supseteq \dots \supseteq \bar{\Theta}_H$. Given a volume measure, it follows $\text{Vol } \Theta_0 \geq \text{Vol } \Theta_1 \geq \text{Vol } \Theta_2 \geq \dots \geq \text{Vol } \bar{\Theta}_H$. Thus, the volume of the hypothesis space is at least not increasing along with user corrections. It is hoped that the volume of search space is strictly decreasing, such that new θ_{i+1} has a very good chance of falling inside $\bar{\Theta}_H$, which means a successful safety alignment between the robot and human. We will later (in Section V) theoretically show that the above *Safe MPC Alignment* method, within finite interactions K , will either

- (I) surely have $\theta_i \in \bar{\Theta}_H \subset \Theta_H$, $i < K$, or
- (II) declare the failure due to misspecification ($\bar{\Theta}_H \cap \Theta_0 = \emptyset$)

Also in Section V, we will provide implementation details for the above hypothesis space cutting procedure.

C. Properties and Geometric Interpretations

In this session, we present some properties and the geometric interpretations for the proposed safe MPC alignment method. The properties will be used to establish the convergence of the algorithm in the next section.

1) *Piecewise Linearity of Cuts*: Recall the weight-feature parameterization of the safety constraint (5). From (12), we can examine $g_\theta(\xi_{\theta_i}^\gamma) < 0$ is a linear inequality in θ .

Based on the definition of the penalty objective function (2), $\langle \bar{\mathbf{a}}_i, \nabla B(\xi_{\theta_i}^\gamma, \theta) \rangle \leq 0$ is a linear fractional inequality

$$\langle \bar{\mathbf{a}}_i, \nabla J(\xi_{\theta_i}^\gamma) \rangle + \gamma \frac{1}{-g_\theta(\xi_{\theta_i}^\gamma)} \langle \bar{\mathbf{a}}_i, \nabla g_\theta(\xi_{\theta_i}^\gamma) \rangle \leq 0, \quad (14)$$

with a positive denominator $-g_\theta(\xi_{\theta_i}^\gamma) > 0$ due to (12). Multiplying the denominator on both side yields another linear inequality. Formally, we give a lemma here about the piecewise linearity of the cut \mathcal{C}_i in (12).

Lemma 3. $\forall i, \mathcal{C}_i$ in (12) can be expressed as an intersection of two half-spaces in \mathbb{R}^r :

$$\mathcal{C}_i = \{\theta \mid \theta^\top \mathbf{h}_i \leq b_i\} \cap \{\theta \mid \theta^\top \phi(\xi_{\theta_i}^\gamma) < -\phi_0(\xi_{\theta_i}^\gamma)\}, \quad (15)$$

with

$$\mathbf{h}_i = -\langle \bar{\mathbf{a}}_i, \nabla J(\xi_{\theta_i}^\gamma) \rangle \phi(\xi_{\theta_i}^\gamma) + \gamma \frac{\partial \phi}{\partial \mathbf{u}}(\xi_{\theta_i}^\gamma) \bar{\mathbf{a}}_i, \quad (16)$$

$$b_i = \langle \bar{\mathbf{a}}_i, \nabla J(\xi_{\theta_i}^\gamma) \rangle \phi_0(\xi_{\theta_i}^\gamma) - \gamma \langle \bar{\mathbf{a}}_i, \nabla \phi_0(\xi_{\theta_i}^\gamma) \rangle. \quad (17)$$

Proof. Equation (15) can be directly obtained from (12), (2) and (5). This completes the proof. \square

With the lemma above, the intersection $\Theta_{i-1} \cap \mathcal{C}_i$ can be viewed as cutting Θ_{i-1} with the boundary of \mathcal{C}_i which consists of two piecewise hyperplanes:

$$\text{bd } \mathcal{C}_i = \{\theta \mid \theta^\top \mathbf{h}_i = b_i, \theta^\top \phi(\xi_{\theta_i}^\gamma) \leq -\phi_0(\xi_{\theta_i}^\gamma)\} \cup \{\theta \mid \theta^\top \mathbf{h}_i \leq b_i, \theta^\top \phi(\xi_{\theta_i}^\gamma) = -\phi_0(\xi_{\theta_i}^\gamma)\}, \quad (18)$$

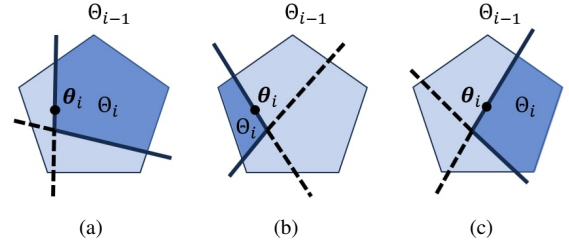


Fig. 5. Illustration of the different choices of θ_i . (a) and (b): When θ_i is chosen near the set boundary, the cut volume (i.e., the volume of the removed hypothesis space) depends on the specific direction of $\text{bd } \mathcal{C}_i$ (i.e., the user-specific directional correction). (c): When θ_i is near the center, the cut volume is large on average regardless of the specific user directional correction.

which is shown in Fig. 4

As the initial hypothesis space $\Theta_0 \in \mathbb{R}^r$ in (10) is a polytope. Iteratively cutting with piecewise hyperplanes yields a series of convex polytopes in \mathbb{R}^r . Consequently, all Θ_i s, $i = 0, 1, 2, \dots$, are convex polytopes.

2) *Relationship between θ_i and $\text{bd } \mathcal{C}_i$* : According to (15), the cut of \mathcal{C}_i depends on robot plan $\xi_{\theta_i}^\gamma$ solved by robot MPC $\pi_{\theta_i}^\gamma$ in (3) with $\theta_i \in \Theta_{i-1}$. This suggests some relationship between θ_i and the boundary \mathcal{C}_i in (18). In fact, the relationship between θ_i and $\text{bd } \mathcal{C}_i$ is given by following lemma.

Lemma 4. $\forall i, \theta_i$ is located on $\text{bd } \mathcal{C}_i$ in (18). Specifically, θ_i satisfies

$$\theta_i^\top \mathbf{h}_i = b_i \quad \text{and} \quad \theta_i^\top \phi(\xi_{\theta_i}^\gamma) < -\phi_0(\xi_{\theta_i}^\gamma) \quad (19)$$

for all $i = 1, 2, \dots$

Proof. See Appendix A-B. \square

The above lemma states $\theta_i \in \text{bd } \mathcal{C}_i$. Its geometric interpretation is in Fig. 5(c): the piecewise cut of \mathcal{C}_i always passes θ_i . This suggests that the choice of $\theta_i \in \Theta_{i-1}$ is critical in the learning process: it directly affects the position of the cut $\text{bd } \mathcal{C}_i$ and consequently the volume to be cut out. Thus, it is important to choose a good $\theta_i \in \Theta_{i-1}$ such that a large hypothesis space is removed after each cut.

We here briefly discuss the implication of different choices of $\theta_i \in \Theta_{i-1}$. When choosing θ_i near the boundary of Θ_{i-1} , as shown in Fig. 5(b) and Fig. 5(a), the removed volume of the hypothesis space depends on the specific direction of cut $\text{bd } \mathcal{C}_i$. Since the direction of the cut $\text{bd } \mathcal{C}_i$ will be eventually dependent upon the user's correction direction according to (18), the removed volume of the hypothesis space can be relatively small, as in Fig. 5(b), or large, as in Fig. 5(a), depending on the specific direction of the correction applied by the user.

As the specific direction of user correction is hard to assume, one can intuitively see that one good choice of $\theta_i \in \Theta_{i-1}$ will be near the center of Θ_{i-1} . As such, we can ensure an averaged large cut of the hypothesis space regardless of the direction of $\text{bd } \mathcal{C}_i$, as shown in Fig. 5(c). We will rigorously discuss the centering choice of θ_i and the guarantee for volume reduction rate of the hypothesis space in the next section.

V. IMPLEMENTATION DETAILS AND MAIN RESULTS

In this section, we will present the details for how to select $\theta_i \in \Theta_{i-1}$ at each iteration i of the hypothesis space cutting in our proposed Safe MPC Alignment algorithm. Based on the preceding geometric intuition, our choice of θ_i is to achieve a large averaged reduction rate for hypothesis space volume given human directional corrections. The reduction rate enables us to establish an exponential convergence of the learning process. As a result, we can find an upper bound of total user corrections to guarantee the success of learning, i.e., $\theta_i \in \Theta_H$, or identify the misspecification of hypothesis space.

A. The Choice of θ_i

As discussed previously, θ_i needs to be picked from the "center" of Θ_{i-1} in the proposed algorithm. An apparent option is to choose the mass center of Θ_{i-1} . However, computing the centroid of a polytope can be #P-Hard [56]. The methods, such as Hit-And-Run algorithm [57], which estimate the mass center by sampling, also suffer from the high sample complexity, thus are impractical in our online real-time setting. In [58], the authors provide another method to choose the center of a polytope using a set of inscribed balls, but it lacks of the guarantee of the volume reduction rate. For computational efficiency and guaranteed convergence, we will use the center of the Maximum Volume Ellipsoid (MVE) inscribed in the convex set Θ_{i-1} as θ_i , shown in Fig. 6.

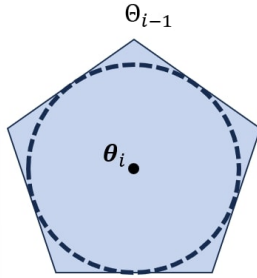


Fig. 6. θ_i is chosen as the center of MVE of Θ_{i-1} (2D example).

Definition 1 (Maximum Volume inscribed Ellipsoid (MVE) [59]). *The MVE of a given convex set $\Theta \subset \mathbb{R}^r$ is defined as the image of the unit ball under an affine transformation*

$$\mathcal{E} = \{\bar{H}\theta + \bar{\mathbf{d}} \mid \|\theta\|_2 \leq 1\}. \quad (20)$$

The affine transformation parameter $\bar{H} \in \mathbb{S}_{++}^r$ ($a \ r \times r$ positive definite matrix), and $\bar{\mathbf{d}} \in \mathbb{R}^r$ is called the center of \mathcal{E} . $\bar{H}, \bar{\mathbf{d}}$ are determined via the following optimization problem for the volume of the ellipsoid $\det H$:

$$\begin{aligned} \bar{H}, \bar{\mathbf{d}} = \arg \max_{H \in \mathbb{S}_{++}^r, \mathbf{d}} \quad & \log \det H \\ \text{s.t.} \quad & \sup_{\|\theta\|_2 \leq 1} \mathbb{1}_{\Theta}(H\theta + \mathbf{d}) \leq 0 \end{aligned}, \quad (21)$$

where the indicator function $\mathbb{1}_{\Theta}(\theta) = 0$ for $\theta \in \Theta$ and otherwise $\mathbb{1}_{\Theta}(\theta) = +\infty$. Specifically, when $\mathbb{1}_{\Theta}$ is a polytope $\{\theta^T \mathbf{h}_i \leq b_i, i = 1, \dots, m\}$, the problem can be converted to a convex optimization problem with m constraints:

$$\begin{aligned} \bar{H}, \bar{\mathbf{d}} = \arg \min_{H \in \mathbb{S}_{++}^r, \mathbf{d}} \quad & \log \det H^{-1} \\ \text{s.t.} \quad & \|H\mathbf{h}_i\|_2 + \bar{\mathbf{d}}^T \mathbf{h}_i \leq b_i, i = 1, \dots, m \end{aligned}. \quad (22)$$

In the *Safe MPC Alignment* algorithm, by the above definition, let \mathcal{E}_{i-1} denote the MVE of Θ_{i-1} and $\bar{\mathbf{d}}_{i-1}$ denote the center of \mathcal{E}_{i-1} . Then, the choice of θ_i is

$$\theta_i = \bar{\mathbf{d}}_{i-1}. \quad (23)$$

Given Θ_{i-1} a convex polytope, the optimization problem (21) can be solved efficiently by convex programming (22).

B. Result 1: Finite Iteration Convergence

In this section, we give the main result that, when using the choice of $\theta_i = \bar{\mathbf{d}}_{i-1}$ mentioned above, the *Safe MPC Alignment* algorithm can converge in a finite number of iterations to find $\theta_H \in \Theta_H \subset \Theta$. This result comes from the fact that the volume reduction rate after each hypothesis space cut is upper bounded, as formally stated below.

Lemma 5. *In the Safe MPC Alignment algorithm, with θ_i as the center $\bar{\mathbf{d}}_{i-1}$ of MVE of Θ_{i-1} , one has*

$$\frac{\text{Vol}(\Theta_i)}{\text{Vol}(\Theta_{i-1})} \leq 1 - \frac{1}{r}. \quad (24)$$

for all $i = 1, 2, 3, \dots$ and any enclosure volume measure Vol .

Proof. See Appendix A-C. \square

The lemma above asserts an upper bound of the volume of the updated hypothesis space $\text{Vol}(\Theta_i)$ relative to the previous volume. With the above result, we can now establish the finite iteration convergence of the proposed *Safe MPC Alignment*, stated below.

Theorem 1 (Successful learning in finite iterations). *In the Safe MPC Alignment algorithm, θ_i is selected as the center $\bar{\mathbf{d}}_{i-1}$ of MVE of Θ_{i-1} , $i = 1, 2, 3, \dots$. If $\Theta_H \subset \Theta_0$, the algorithm will terminate successfully within*

$$K = \left\lceil \frac{\ln \frac{\tau_r \rho_H^r}{\text{Vol}(\Theta_0)}}{\ln(1 - \frac{1}{r})} \right\rceil. \quad (25)$$

iterations, where ρ_H is the radius of a ball contained within Θ_H and τ_r is the volume of a unit ball in \mathbb{R}^r space. That is, there exists $i < K$, such that $\theta_i \in \Theta_H \subset \Theta$.

Proof. See Appendix A-D. \square

The above main result asserts a maximum iteration count for the proposed algorithm to find $\theta_i \in \Theta_H$. In other words, within K rounds of human corrections, the robot can successfully learn a safety set intended by the user. The above result requires a pre-set of ρ_H^r , which is the radius of a ball contained in Θ_H . Since the size of Θ_H is unknown in practice, $\rho_H > 0$ can be interpreted as an underestimated size of the unknown user intent set Θ_H . It also serves as a termination threshold for learning convergence: a smaller ρ_H can lead to a more concentrated learned θ .

However, the finite iteration convergence certificate in Theorem 1 comes with a prerequisite: $\bar{\Theta}_H \in \Theta_0$ has to be satisfied in the first place in the Safe MPC Alignment algorithm. Although such a condition can be achieved by empirically choosing Θ_0 large enough to contain all possible $\bar{\Theta}_H$ (10), it is also desired to have a systematic way to detect the hypothesis misspecification. In the next session, we will discuss the identification of hypothesis misspecification, where such condition is not met.

C. Result 2: Hypothesis Misspecification Declaration

We consider the case of hypothesis space misspecification, where $\bar{\Theta}_H \cap \Theta_0 = \emptyset$. In this case, no $\theta \in \Theta_0$ can account for the user intended safety (4). As mentioned in [54], [60], this kind of gap between hypothesis space and true human model can lead to undesired behavior of the robot. The following result states the proposed Safe MPC Alignment algorithm can automatically certify the misspecification of the initial hypothesis space.

Theorem 2 (Identifying misspecification). *In the Safe MPC Alignment algorithm, θ_i is selected as the center $\bar{\mathbf{d}}_{i-1}$ of MVE of Θ_{i-1} , $i = 1, 2, 3, \dots$. If $\bar{\Theta}_H \cap \Theta_0 = \emptyset$, the algorithm converges to a set Θ^* as $i \rightarrow \infty$, such that $\text{Vol}(\Theta^*) = 0$ and $\Theta^* \cap \text{int } \Theta_0 = \emptyset$.*

Proof. See Appendix A-E. \square

The above result states that, when the initial hypothesis space is misspecified, $\bar{\Theta}_H \cap \Theta_0 = \emptyset$, the Safe MPC Alignment algorithm will finally converge to a set of zero volume on the boundary of the initial hypothesis space Θ_0 .

The above theorem inspires us to empirically identify the misspecification by examining the position of MVE centers during the converging process: if after the maximum iteration step $K - 1$ in (25), the MVE center θ_{K-1} is very close to the boundary of initial hypothesis set (10), there is likely hypothesis space misspecification and further adjustment on initial hypothesis space should be made. See Fig. 7.

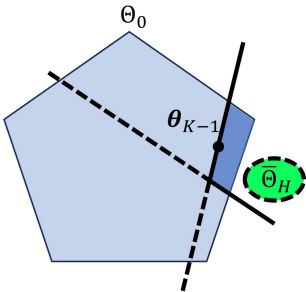


Fig. 7. When there is misspecification, the Safe MPC Alignment algorithm will converge to some point on the boundary of Θ_0 . So we can use the distance from θ_{K-1} to the boundary as a signal for misspecification.

Specifically, recall (10) that Θ_0 is a box with bounding vector c_l, c_h , we can pre-define a small threshold ϵ to examine

every entry of θ_{K-1} and identify possible misspecification. If θ_{K-1} satisfies the criterion

$$\min_j |c_l[j] - \theta_{K-1}[j]| \leq \epsilon \text{ or } \min_j |c_h[j] - \theta_{K-1}[j]| \leq \epsilon, \quad (26)$$

it means θ_{K-1} is very close to the boundary of Θ_0 . We consider there is likely misspecification in this case.

D. Detailed Algorithm of Safe MPC Alignment

With the detailed centering choice method of θ_i as well as the main results on convergence and misspecification, we can establish the full safe MPC alignment. With initializing Θ_0 and pre-define a termination threshold ρ_H , three steps in the hypothesis space cutting are executed until user satisfies robot motion or the iteration count reaches the maximum count K in (25). Note that during the execution of the MPC policy, $\pi_{\theta_i}^\gamma$, the human can perform emergency stopping and reset the robot's state, which corresponds to Section III-C3.

When reaching and exist after $K - 1$ iterations, the algorithm checks the misspecification by (26). The Safe MPC Alignment algorithm with misspecification identification is presented in the Algorithm 1.

Algorithm 1: Safe MPC Alignment Algorithm

Initialization: Parameterized constraint g_θ , initial hypothesis space Θ_0 , termination threshold ρ_H (i.e., approximate radius of $\bar{\Theta}_H$), $i = 1$

Compute maximum correction count K from ρ_H in (25);

while $i < K$ **do**

 Choose $\theta_i \in \Theta_{i-1}$ using (23);

 Robot executes $\pi_{\theta_i}^\gamma$;

if Human provides directional correction \mathbf{a}_{k_i} **then**

 Generate $\bar{\mathbf{a}}_i$ using (6);

 Calculate the cutting set C_i using (15);

 Update hypothesis space $\Theta_i = \Theta_{i-1} \cap C_i$;

$i \leftarrow i + 1$;

else if Human triggers emergency stop **then**

 Human restarts robot from safe region.;

else if Human user is satisfied **then**

return θ_i ;

end

if θ_{K-1} satisfies (26) **then**

return misspecification failure;

else

return θ_{K-1}

end

VI. NUMERICAL EXAMPLE AND USER STUDY IN SIMULATION GAMES

In this section, we will first evaluate the proposed *Safe MPC Alignment* method using a numerical example with simulated human corrections knowing ground-truth safety constraints. Then, we will test the performance of the methods in two user studies using two simulation games developed based on MuJoCo [61]. We consider two typical robot tasks. One is a drone navigation task and the other a 7-DOF robot arm reaching task. In both user studies, the robot is controlled by an MPC

controller and human participants provide simulation robots with real-time correction instructions through a keyboard. The objective of each game is to teach a robot to successfully learn a safe MPC to move through an unknown safety-critical environment.

The organization in this section is as follows: Subsection VI-A presents the numerical evaluation and its analysis. Subsections VI-B and VI-C describe the setting of the two developed simulation games used in our user study. Subsection VI-D details the study procedure and the recruitment of human users. The results of the user studies and some analysis are given in VI-E. Please access the accompanying codes at <https://github.com/asu-iris/Safe-MPC-Alignment>.

A. Numerical Example

1) *Environment Setup*: We use the safe control of an inverted pendulum as the numerical example. The dynamics equation of an inverted pendulum is

$$\ddot{\alpha} = \frac{3}{ml^2} \left(-\frac{1}{2}mgl \sin \alpha + u - d\dot{\alpha} \right), \quad (27)$$

with α being the angle between the pendulum and the direction of gravity, $g = 10\text{m/s}^2$ the gravity constant, u the pivot torque, $m = 1\text{kg}$, $l = 1\text{m}$ and $d = 0.4$ being the length, inertia, and dampening of the pendulum. We set the system state as $\mathbf{x} = [\alpha, \dot{\alpha}]^T$ and discretize (27) by the Euler method with $\Delta t = 0.02\text{s}$. A zero-mean Gaussian noise with covariance $\Sigma = \text{diag}(1, 4) \times 10^{-5}$ is added to \mathbf{x} at each control step to simulate the state noise. The task is to control the pendulum to the target $\mathbf{x}^* = [\pi, 0]^T$. We additionally pose the following unknown state affine constraint to the motion of the pendulum

$$0.6\alpha + \dot{\alpha} = \boldsymbol{\theta}^H \mathbf{x} \leq 3, \quad (28)$$

where $\boldsymbol{\theta}^H = [0.6, 1]^T$ is to be learned.

In Safe MPC formulation (1), we set $T = 40$, the step cost $c(\mathbf{x}_t, u_t)$ and terminal cost $h(\mathbf{x}_T)$

$$\begin{aligned} c(\mathbf{x}_t, u_t) &= Qu_t^2 \\ h(\mathbf{x}_T) &= (\mathbf{x}_T - \mathbf{x}^*)^T R(\mathbf{x}_T - \mathbf{x}^*), \end{aligned} \quad (29)$$

respectively, with $Q = 0.1$ and $R = \text{diag}(25, 10)$.

To ensure the safe MPC rollout trajectory to satisfy a global constraint, it is sufficient to learn a safety constraint in safe MPC defined on the closest controllable state. Thus, in (1), we aim to define and learn a constraint defined on the first controlled state:

$$g_{\boldsymbol{\theta}}(\boldsymbol{\xi}) = -3 + \boldsymbol{\theta}^T \mathbf{x}_1. \quad (30)$$

In asymptotic MPC approximation, we set $\gamma = 0.1$.

Suppose the user intent set $\bar{\Theta}_H = \{\boldsymbol{\theta} \mid \|\boldsymbol{\theta} - \boldsymbol{\theta}_H\| \leq 0.02\}$. Then, simulated human corrections \mathbf{a} can be generated as follows: when the system is running near the human safety boundary, i.e., $g_{\boldsymbol{\theta}_H}(\boldsymbol{\xi}_{\boldsymbol{\theta}}^\gamma) > -\epsilon_g$ ($\epsilon_g = 0.25$ here), a correction \mathbf{a} can be generated in probability $p = 0.3$ using the first element of the signed gradient vector $\text{sign}(-\nabla B(\boldsymbol{\xi}_{\boldsymbol{\theta}}^\gamma, \boldsymbol{\theta}_H))$. Recall that $B(\boldsymbol{\xi}, \boldsymbol{\theta})$ is the barrier function in (2). It is trivial to verify that this correction \mathbf{a} has positive product with $-\nabla B(\boldsymbol{\xi}_{\boldsymbol{\theta}}^\gamma, \boldsymbol{\theta}_H)$, and by definition it is applied to a safe trajectory $\boldsymbol{\xi}_{\boldsymbol{\theta}}^\gamma$. The both

hypotheses in section IV-A is then satisfied, and a can be used as a valid human correction.

When the system state violates $g_{\boldsymbol{\theta}_H}(\boldsymbol{\xi}_{\boldsymbol{\theta}}^\gamma) \leq 0$ or it is near the target, the pendulum state is uniformly randomly reset between $[0, 0]^T$ and $[\frac{2\pi}{3}, 3]^T$. Simulated human correction will continue to be applied until the learned parameters $\boldsymbol{\theta}_i$ fall in $\bar{\Theta}_H$, which terminates one trial.

2) *Convergence Analysis*: In the first session, we evaluate the convergence of the learning algorithm without hypothesis misspecification. In Algorithm 1, we set the initial hypothesis Θ_0 with box boundaries $\mathbf{c}_l = [-6, -6]^T$ and $\mathbf{c}_h = [2, 2]^T$; thus Θ_0 includes $\bar{\Theta}_H$. The initial value of $\boldsymbol{\theta}_1$ is set as $[-2, -2]^T$ (i.e., the center of Θ_0).

With simulated human corrections, we run Algorithm 1 and track the update of $\boldsymbol{\theta}_i$ after every correction. $\boldsymbol{\theta}_i$ falls in the intention set $\bar{\Theta}_H$ after 14 corrections, triggering the termination of learning. We then respectively evaluate each history $\boldsymbol{\theta}_i$ by using it as the MPC constraint parameter to control the system starting from $\mathbf{x} = [0, 0]^T$. We plot the corresponding MPC rollout trajectory in $(\alpha, \dot{\alpha})$ phase plot in Fig. 8. The affine ground-truth constraint (28) and the corresponding learned constraints $g_{\boldsymbol{\theta}_i}$ are also shown in Fig. 8. From Fig. 8, we can conclude that the ground-truth constraint can be successfully recovered from the simulated corrections. The precision of this recovery is very high and the learned and ground-truth safety boundary almost overlap.

To further analyze the convergence of the algorithm, we run the algorithm for 10 times, all of which terminate after 12-17 corrections. In each run, we keep track of the following two metrics over correction count, shown in Fig. 9.

M1 (left panel of Fig. 9): The logarithm volume measure of the solved MVE $\log \det \bar{H}$ in (21). This provides a lower bound of Θ_i to show the exponential convergence property.

M2 (right panel of Fig. 9): The euclidean distance between learned parameter $\boldsymbol{\theta}_i$ and $\boldsymbol{\theta}_H$, i.e. $\|\boldsymbol{\theta}_i - \boldsymbol{\theta}_H\|_2$. This suggests the similarity between the learned constraint and the ground-truth constraint, see Fig. 9.

From Fig. 9, we can conclude the proposed algorithm is

- (I) Fast-converging. During learning, the logarithm volume $\log \det \bar{H}$ has near-linear decreasing property. This observation is consistent with the exponential convergence in theory stated in Lemma 5.
- (II) Correction-efficient. During learning, $\|\boldsymbol{\theta}_i - \boldsymbol{\theta}_H\|_2$ converges to the value lower than 0.02 within 17 corrections. By using 2D area as a volume measure, we can compute the upper bound of correction count by Theorem 1 :

$$\ln \frac{\tau_r \rho_H^r}{\text{Vol}(\Theta_0)} / \ln(1 - \frac{1}{r}) = 17.28. \quad (31)$$

This suggests that the algorithm is guaranteed to converge within finite $K = 17$ corrections, this is consistent with the observations in the experiment.

3) *Result Analysis for Misspecification Case*: To analyze the performance of the proposed algorithm in misspecification cases, we set the initial hypothesis Θ_0 as $\hat{\mathbf{c}}_l = [-1, -1]^T$ and $\hat{\mathbf{c}}_h = [0.8, 0.8]^T$ which does not contain $\bar{\Theta}_H$. In this setting, the algorithm automatically stops after 7th correction. The path of $\boldsymbol{\theta}_i$, $i = 1, \dots, 8$ is shown in Fig. 10. In Fig. 10, $\boldsymbol{\theta}_i$

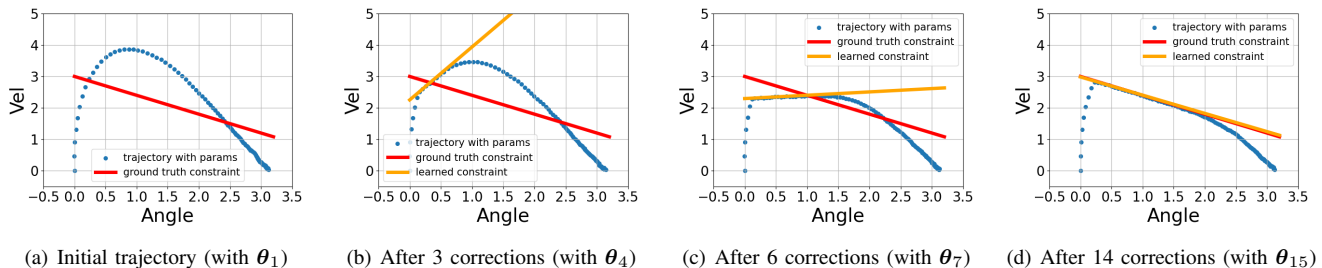


Fig. 8. The pendulum rollout trajectory at different correction interactions: (a) trajectory with θ_1 , (b) with θ_4 , (c) with θ_7 , (d) with θ_{15} . The learned constraint with θ_1 is omitted since it covers the whole first quadrant. As the learning proceeds, the learned constraint boundary (orange line) converges to the ground-truth constraint boundary (red line). When the learning process terminates, the learned and ground-truth constraint boundaries almost overlap, suggesting the success of constraint learning from corrections.

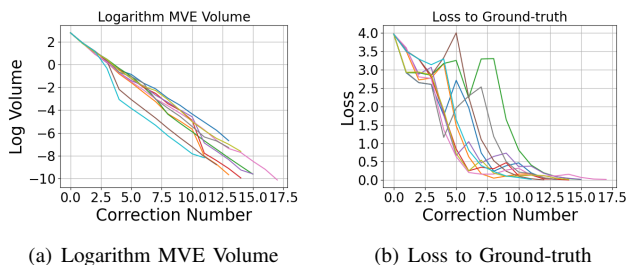


Fig. 9. (a) The plot of $\log \det \bar{H}$ with respect to correction numbers. In all algorithm runs, the plot shows the near-linear decrease of the logarithm volume, suggesting the exponential decrease of the volume of MVE of the hypothesis spaces, as asserted in Theorem 1. (b) The plot of the parameter estimation error $\|\theta_i - \theta_H\|_2$ versus correction numbers. In all runs, the parameter estimation error can converge to a value lower than 0.02 within 17 corrections.

is continuously moving towards the boundary of the initial hypothesis space Θ_0 . This fact verifies Theorem 2 and justifies the proposed method is capable of misspecification detection.

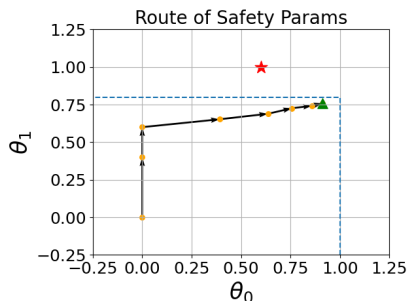


Fig. 10. Illustration of misspecification case. The blue dashed lines are the boundary of Θ_0 . θ_i , $i = 1, \dots, 7$ is shown in the orange dots in one run. Black arrows show the update directions of θ_i s. The center of the ground-truth intent set is marked as the red star, and the θ_8 at the termination of learning is marked as the green triangle. When misspecification happens, θ will converge toward the boundary of Θ_0 , as stated by Theorem 2.

B. Drone Navigation Game

1) *Environment Setup*: As shown in Fig. 11, the goal of this drone navigation game is let a human user to teach a drone to successfully navigate through a narrow gate (rectangle frame in yellow) whose position is unknown, given different flying target positions (shown in yellow points behind the gate). The

drone starts from $[x_{\text{init}}, y_{\text{init}}, z_{\text{init}}]^T$ with $x_{\text{init}} = 0.1$, $z_{\text{init}} = 0.5$, and y_{init} uniformly randomly in an interval $[4, 6]$. The starting quaternion $\mathbf{q}_{\text{init}} = [1, 0, 0, 0]^T$. We set three different target positions at $[19, 1, 9]^T$, $[19, 5, 9]^T$ and $[19, 9, 9]^T$, with target quaternion $[1, 0, 0, 0]^T$. For the narrow gate (yellow rectangle), both its size and position are unknown, and one only roughly know its x position $x_{\text{gate}} \approx 10.0$. The drone navigation game is developed using MuJoCo physics engine [61].

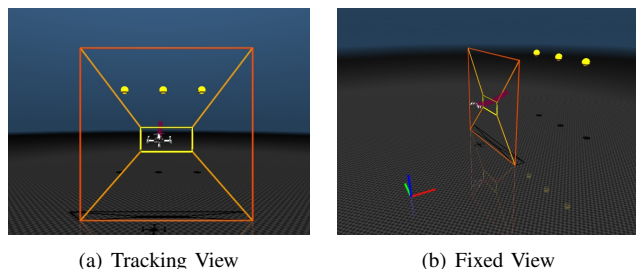


Fig. 11. Drone Navigation Game. (a) The tracking view seen by the user in the drone user study. (b) The fixed view seen by the user in the drone user study. Users can precept the motion of the drone in 3D space with the help of these two views. The xyz -axis (red, green, and blue lines), the gate (yellow bars for the edge, orange bars for the outer frame), the drone (white robot model), the local plan outputted from MPC (red curve) and current motion target (yellow balls) are visible to users. In runtime, the user will see one target at a time.

Since the location of the gate is unknown, the drone needs to learn a safety constraint in its safe MPC policy with humans guidance in order to successfully fly through the gate. In the drone MPC policy (1), the dynamics and its parameters are set following ([7]); and we generically set the constraint function $g_{\theta}(\xi)$ using a set of N Gaussian radial basis functions (RBFs)

$$g_{\theta}(\xi) = \phi_0 + \sum_{i=1}^N \theta_i \phi_i(\xi). \quad (32)$$

As discussed in Section III-C4, we fix $\phi_0 = -1$ to avoid learning ambiguity, and use $N = 20$ temporally accumulated RBFs defined as

$$\phi_i(\xi) = \sum_{t=0}^T \beta_t \text{RBF}_i(\mathbf{x}_t), \quad (33)$$

where β_t is a weighting factor to control or balance the immediate and future constraint satisfaction of robot MPC control. If one emphasizes instant safety, more weights will be given to the initial time step. In our implementation, inspired

by the practice in RL, we choose an exponentially decaying β_t starting at $t = 5$, i.e. $\beta_t = 0$, $t < 5$ and $\beta_t = 0.9^{t-5}$, $t \geq 5$ to achieve better predictive safety performance. In (33), each Gaussian RBF is defined as

$$\text{RBF}_i(\mathbf{x}_t) = \begin{cases} \exp(-\epsilon^2 \|r_{xy,t} - c_{xy,i}\|^2), & i = 1, \dots, 10 \\ \exp(-\epsilon^2 \|r_{xz,t} - c_{xz,i}\|^2), & i = 11, \dots, 20 \end{cases} \quad (34)$$

Here, the variables $r_{xy,t} = [r_{x,t}, r_{y,t}]^\top$ and $r_{xz,t} = [r_{x,t}, r_{z,t}]^\top$ with r_x, r_y, r_z from \mathbf{x}_t . The i th center $c_{xy,i} = [c_{x,i}, c_{y,i}]^\top$ or $c_{xz,i} = [c_{x,i}, c_{z,i}]^\top$ is defined with $c_{x,i} = x_{\text{gate}} = 9.8$, $c_{y,i}$ and $c_{z,i}$ are evenly chosen on interval $[0, 10]$. We set $\epsilon = 0.45$. The initial hypothesis space Θ_0 for possible θ in (32) is set as $\mathbf{c}_l = [-80, \dots, -80]^\top$ and $\mathbf{c}_h = [100, \dots, 100]^\top$. γ is 50. This initialization blocks the drone from advancing to the gate at the beginning of the game, leading to conservative behavior in the learning process. The drone will proceed toward the gate after few corrections.

2) *Human Correction Interface*: The motion of the drone is rendered in two camera views in MuJoCo visualization (Fig. 11) for better human perception: one is the first-person view tracking the drone, the other a third-person fixed view. The gate, the current MPC planning solution, and the target position are visible to the users.

Human users apply corrections to the drone via a keyboard during the drone flying. The user is informed of the mappings between the key press and the corresponding correction in the game, listed in Table I. The safety constraint (32) in the drone's MPC policy is immediately updated once a user correction is detected. When the user presses "ENTER", the drone is reset to the initial position and the target will also change.

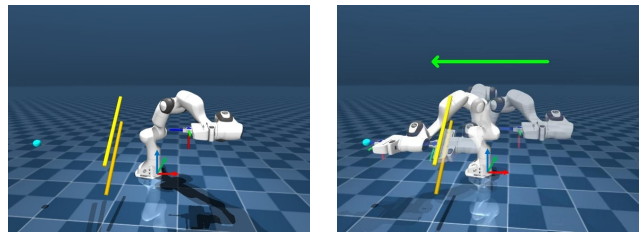
TABLE I
KEYBOARD COMMANDS IN UAV USER STUDY

| Key | Correction | Interpretation |
|---------|-------------------------|---|
| "up" | $[-1, 0, 1, 0]^\top$ | Go forward (adding positive y-axis torque) |
| "down" | $[1, 0, -1, 0]^\top$ | Go backward (adding negative y-axis torque) |
| "left" | $[0, 1, 0, -1]^\top$ | Go left (adding negative x-axis torque) |
| "right" | $[0, -1, 0, 1]^\top$ | Go right (adding positive x-axis torque) |
| "shift" | $[1, 1, 1, 1]^\top$ | Go up (increasing all thrusts) |
| "ctrl" | $[-1, -1, -1, -1]^\top$ | Go down (decreasing all thrusts) |
| "enter" | N/A | Reset robot position and switch target. |

C. Franka Constrained Reaching Game

1) *Environment Setup*: As shown in Fig. 12, the goal of the Franka constrained reaching game is to teach a simulated Franka robot arm such that its gripper hand successfully reaches different target positions (shown in cyan ball) through a narrow slot (shown by two yellow bars) with unknown position or geometry. Specifically, the arm starts at a configuration in which the end-effector position $\mathbf{r}_{\text{init}} = [0.22, -0.5, 0.48]^\top$ and altitude $q_{\text{init}} = [0, -0.707, 0, 0.707]^\top$. The reaching target position \mathbf{r}^* will be dynamically chosen from three options $[-0.6, -0.5, 0.4]^\top$, $[-0.6, -0.5, 0.5]^\top$, $[-0.6, -0.5, 0.6]^\top$. The reaching target attitude is $\mathbf{q}^* = [0, -0.707, 0, 0.707]^\top$. The slot size and position are unknown except its rough x-position which is $x_{\text{slot}} \approx -0.15$.

We adopt a two-level control scheme, where a safe MPC policy (high-level) is defined for the end effector, which



(a) Starting Configuration (b) Motion Illustration

Fig. 12. Franka Constrained Reaching Game. (a) The starting configuration of the arm in the user study. RGB arrows denote the world xyz -frame. (b) Illustration of one successful reach by adjusting the position and altitude of the gripper, long green arrow denotes the motion direction. Users can precept the motion of the robot arm in 3D space by adjusting the view. The bars, the robot arm, and current motion target (cyan ball) are all visible to users.

generates the desired velocity for a given low-level operational space controller to track. In the safe MPC policy, we model the end-effector dynamics as

$$\begin{aligned} \dot{\mathbf{r}} &= \mathbf{v}^d, \\ \dot{\mathbf{q}} &= \frac{1}{2} \Omega(R^\top(\mathbf{q})\mathbf{w}^d)\mathbf{q}, \end{aligned} \quad (35)$$

where \mathbf{r} and \mathbf{q} is the position and the quaternion of the arm end-effector in the world frame. $R^\top(\mathbf{q})$ is the rotation matrix from the end-effector frame to the body frame. $\Omega(\cdot)$ is the matrix operator of the angular velocity for quaternion multiplication. Define the robot state and control input

$$\mathbf{x}_t = [\mathbf{r}_t, \mathbf{q}_t] \in \mathbb{R}^7, \quad \mathbf{u}_t = [\mathbf{v}_t^d, \mathbf{w}_t^d] \in \mathbb{R}^6, \quad (36)$$

respectively.

The above end-effector dynamics is discretized with $\Delta t = 0.1\text{s}$. In (1), the control horizon is $T = 20$. Let $\mathbf{x}^* = [\mathbf{r}^* \ \mathbf{q}^*]$ denote the target end-effector pose. The step cost $c(\mathbf{x}_t, \mathbf{u}_t)$ and terminal cost $h(\mathbf{x}_T)$ in (1) is set to

$$\begin{aligned} c(\mathbf{x}_t, \mathbf{u}_t) &= (\mathbf{r}_t - \mathbf{r}^*)^\top Q_r (\mathbf{r}_t - \mathbf{r}^*) + k_q \text{diff}(\mathbf{q}_t, \mathbf{q}^*) \\ &\quad + \mathbf{v}_{I,t}^\top R_v \mathbf{v}_{I,t} + \mathbf{w}_{I,t}^\top R_w \mathbf{w}_{I,t}, \\ h(\mathbf{x}_T) &= (\mathbf{r}_T - \mathbf{r}^*)^\top S_r (\mathbf{r}_T - \mathbf{r}^*) + \mu_q \text{diff}(\mathbf{q}_T, \mathbf{q}^*). \end{aligned} \quad (37)$$

In this game, the cost parameters are set as $Q = \text{diag}(2, 2, 2)$, $k_q = 1$, $R_v = \text{diag}(30, 30, 1)$, $R_w = \text{diag}(0.85, 0.85, 0.85)$, $S_r = \text{diag}(80, 80, 80)$, and $\mu_q = 60$. The output of the MPC controller is sent to the low-level controller to track.

Similar to Section VI-B, to constrain r_z and \mathbf{q} for proper height and tilt in order to pass through the slot. We use a set of $N = 20$ Gaussian radial basis function (RBFs) to parameter the safety constraint:

$$g_\theta(\boldsymbol{\xi}) = \phi_0 + \sum_{i=1}^N \theta_i \phi_i(\boldsymbol{\xi}), \quad (38)$$

with

$$\phi_i(\boldsymbol{\xi}) = \sum_{t=0}^T \beta_t \text{RBF}_i(\mathbf{x}_t), \quad \text{and} \quad (39)$$

$$\text{RBF}_i(\mathbf{x}_t) = \begin{cases} \sigma(r_{x,t}) k_z \exp(-\epsilon_z^2 (r_{z,t} - c_{z,i})^2), & i=1, \dots, 10 \\ \sigma(r_{x,t}) \exp(-\epsilon_q^2 \text{diff}(\mathbf{q}_t, \mathbf{q}_{c,i})), & i=11, \dots, 20 \end{cases} \quad (40)$$

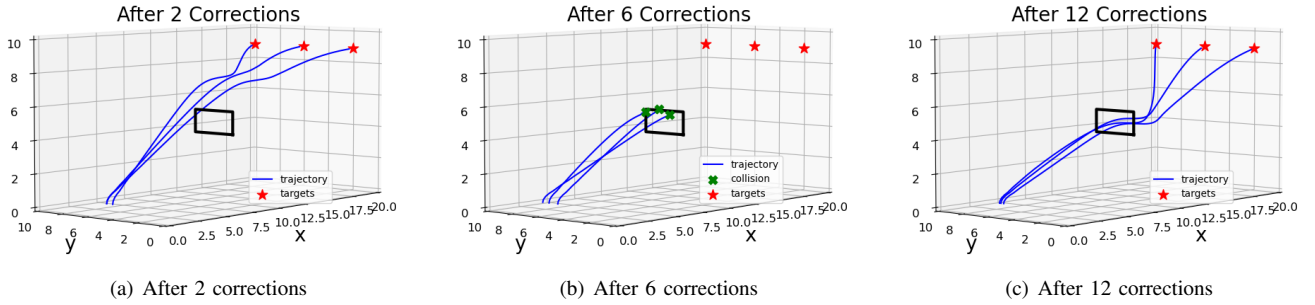


Fig. 13. Illustrations of the drone MPC rollout trajectory after $k = 2, 6, 12$ corrections. The red stars denote the target positions and the blue curves denote the trajectories. The gate is drew in black lines and collision is denoted by green crosses. User's corrections typically lower the flying drone to make it pass through the gate.

Here, k_z is used to balance the scaling between position and orientation RBFs, $\sigma(r_{x,t})$ is defined as

$$\sigma(r_{x,t}) = \text{sigmoid}\left(50\left((r_{x,t} - x_{\text{slot}})^2 - \left(\frac{w}{2}\right)^2\right)\right), \quad (41)$$

which is used to constrain the RBF_{*i*} only taking effect around x range $[x_{\text{slot}} - \frac{w}{2}, x_{\text{slot}} + \frac{w}{2}]$ (recall slot's x location, slot, is a approximate value). In the above definition, $w = 0.3$, $k_z = 0.05$, $\epsilon_z = 12$ and $\epsilon_q = 1.8$. The center of positional RBF, $c_{z,i}$, is evenly chosen on interval $[0, 1]$, and the center of orientation RBF, $\mathbf{q}_{c,i}$, is generated by $(\cos \frac{\alpha}{2}, \sin \frac{\alpha}{2}, 0, 0) * \mathbf{q}_{\text{init}}$ with α evenly choosen from $[-\pi/4, 3\pi/4]$ to make sure $\mathbf{q}_{c,i}$ covers all possible orientations. $\beta_t = 0.9^t$ if $t < 5$ and 0 otherwise. The bounds of the initial hypothesis space Θ_0 is set to $\mathbf{c}_l = [-3, \dots, -3]^T$ and $\mathbf{c}_h = [5, \dots, 5]^T$. γ is set to 1.5. This initialization leads to a conservative MPC policy, preventing the arm from approaching the target at the beginning.

2) *Human Correction Interface*: The motion of the robot arm is rendered in the free-view mode in MuJoCo visualization (Fig. 12), and users can drag to select his/her comfortable view. The slot and the random reaching target are visible to the users.

Human users apply their corrections to the robot arm via a keyboard. Users are informed with the following key mapping between the key press and the corresponding correction in the game. The safety constraint (38) in Franka arm's safe MPC policy is updated immediately once a user correction is detected. When user press "ENTER", the arm is reset to the initial position and the reaching target will also change.

TABLE II
KEYBOARD COMMANDS IN ROBOT ARM USER STUDY

| Key | Correction | Interpretation |
|---------|-------------------------|---|
| "left" | $[0, 0, 0, 0, 0, 1]^T$ | Clock-wise rotation of the gripper |
| "right" | $[0, 0, 0, 0, 0, -1]^T$ | Anti-clock-wise rotation of the gripper |
| "shift" | $[0, 0, 0, -1, 0, 0]^T$ | Go up in world frame |
| "ctrl" | $[0, 0, 0, 1, 0, 0]^T$ | Go down in world frame |
| "Enter" | N/A | Reset robot position and switch target. |

D. Participants, Procedures, and Metrics

1) *Participants*: We recruited 15 participants from the student population of Arizona State University, covering undergraduate, master's, and PhD students with different

backgrounds. Among all participants, 13 are male and 2 female. All participants are novices to the user study. This user study had been reviewed and approved by the Institutional Review Board (IRB) of Arizona State University, and all participants had signed the consent forms.

2) *Procedure*: Each participant was instructed to play the previously developed two simulation games. In each game, each participant plays 10 trials.

In the drone navigation game, a trial is deemed successful when the drone navigates through the gate without collision and successfully reaches different targets 6 consecutive times with the learned safe MPC policy. A trial is deemed failed when there are too many corrections, causing the crash of the MVE solver, or the user believes the robot cannot be corrected anymore and gives up.

In the Franka reaching game, a trial is deemed successful when the robot arm reaches different targets without collision with the slot frame with the learned safe MPC controller. The failure of one trial is determined when there are too many corrections or the user believes the robot cannot be corrected anymore and gives up.

The result of every trial is recorded. Before formally starting the study, every user is instructed about the settings of the game and is given 2 chances for hands-on trying of the environments to get familiar with the keys and commands.

3) *Metrics for Evaluation*: Two major metrics are used to evaluate the performance of the proposed *safe MPC alignment* algorithm in our user study:

- (I) *Success rate*: The overall and individual success rate suggest the **effectiveness** of the proposed method.
- (II) *Numbers of corrections needed for a successful trial*: The averaged number of corrections performed by the users in successful trials is a measure for the **efficiency** of the proposed method. Fewer corrections in successful trials suggest better efficiency in teaching the robot.

E. Result and Analysis

1) *User Study Metrics Report*: For the user study, we report the success rate and correction count in a successful game trial in Table III. Both metrics are averaged across individual users. The success rate is $89.3\% \pm 7.7\%$ for the drone navigation game and $89.3\% \pm 11.2\%$ for the Franka arm constrained

TABLE III
RESULT OF SIMULATED USER STUDY

| Environment | Success Rate | Correction count |
|---------------------|---------------------|------------------|
| Drone navigation | $89.3\% \pm 7.7\%$ | 15.7 ± 10.6 |
| Franka arm reaching | $89.3\% \pm 11.2\%$ | 16.5 ± 6.1 |

reaching game. The number of corrections for a successful trial is 15.7 ± 10.6 for the drone navigation game and 16.5 ± 6.1 for the Franka arm reaching games.

The above result illustrates that the proposed method is effective (i.e., with a high success rate) in enabling a robot to learn a safety constraint for varying tasks (i.e. reaching targets are changing). It also shows the efficiency of the proposed method — successful learning of a safety constraint only requires tens of human corrections. Since this method is online and the user can perform multiple corrections in one robot rollout trajectory, the constraint can be learned to guide the robot to complete safety-critical tasks in a few runs. In Table III, one can note that the drone navigation task has a higher variance in the correction count than the Franka arm reaching task. This could be attributed to the larger motion range and longer task rollout horizon of drone navigation. As a result, in the drone game, the human correction strategies, including the correction position and correction timing, can vary significantly. Such diverse correction strategies can lead to a larger variance of total correction count.

2) *Analysis for Learned Behavior and Learned Constraint:* To demonstrate the learning progress, in Fig. 13 and Fig. 14, we illustratively show the intermediate robot motion at different numbers of human corrections. Fig. 13 shows the flight trajectory of the drone after different numbers of human corrections. Fig. 14 shows the position and altitude of the robot arm’s end effector when passing the slot after the different number of human corrections. From the illustration examples, we can conclude that the learned constraint generally guides the robot to complete the task.

To better understand the learned safety constraint function $g_{\theta}(\xi)$, in Fig. 15, we draw the heat map of the value of $g_{\theta_H}(\xi)$ with θ_H the averaged value of weights learned in all successful trials. In drawing such heat map, since g_{θ_H} is defined by RBFs spreading only on yz -plane, we fix $r_{x,t} = 10$ (recall $x_{\text{gate}} = 9.8$) and $r_{y,t}, r_{z,t}$ are generated by the grid in $[0, 10] \times [0, 10]$ for all states \mathbf{x}_t in ξ . In the heat map, we draw the 0-level contour of g_{θ_H} in the dashed line, which is the learned safety boundary. Also, we plot the yz -plane projection of the gate, which is the black box.

In Fig. 15, we can note the learned safety boundary (corresponding to $g_{\theta_H}(\xi) \leq 0$) is only similar to the top edge of the gate. This is explained by the following reasons. As shown in Fig. 11, the target positions are set higher than the gate, and thus during the learning process, the motion of the drone is always going up, as shown in Fig. 13. As a result, the majority of human directional corrections happen when the drone approaches the top edge of the gate, leaving the learned safety boundary accurate near the top edge of the gate and bottom boundary untouched. It is expected that in order to learn a safety constraint that fully represents the gate frame,

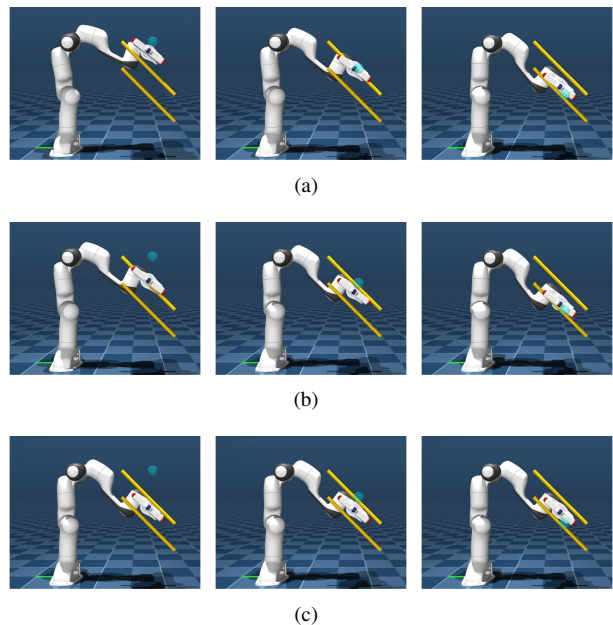


Fig. 14. Illustrations of the robot arm pose when passing the yz -plane of the bars after $k = 4, 8, 17$ corrections. (a): The motion after 4 corrections with three different targets (cyan ball). (b): The motion after 8 corrections. (c): The motion after 17 corrections. The ends of the gripper are denoted with red balls. At the beginning, the gripper cannot pass the slot. But after several corrections, it succeeds in passing the slot for all target positions.

lower target positions should be added so that the drone will receive human corrections near the bottom of the gate.

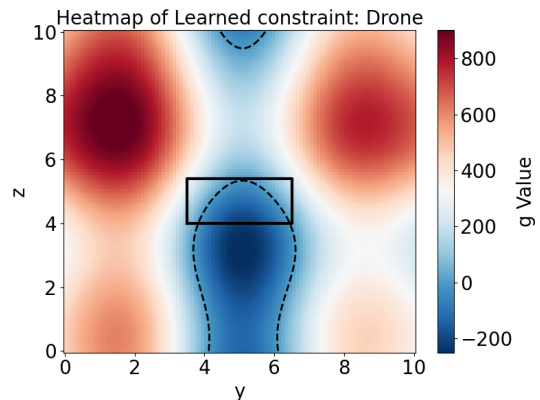


Fig. 15. Heatmap for the learned constraint function in the drone user study. The black solid line denotes the actual position of the gate in yz -frame. The black dashed curve denotes the boundary of the safety zone. Since the target positions are higher than the gate (see Fig. 11), thus during the learning process, the motion of the drone is always going up, as shown in Fig. 13. As a result, the majority of human directional corrections happen when the drone approaches the top edge of the gate, leaving the learned safety boundary accurate near the top edge of the gate and bottom boundary untouched.

VII. USER STUDY IN REAL-WORLD ROBOT EXPERIMENT

In this section, we conduct a user study to evaluate the performance of our safe MPC alignment algorithm using a hardware Franka Research 3 robot experiment. We focus on the task of *mobile liquid pouring*, i.e., the robot performs liquid pouring while moving from one location to another. In certain

scenarios, this kind of task can be safety-critical: for example, if the liquid is corrosive/chemical/toxic, inappropriate mobile pouring will cause safety concerns. The task is challenging because it is hard to manually define a safety constraint for the robot to accomplish liquid pouring without spilling. The Franka robot arm will learn such a safe MPC controller from human physical corrections.

A. Hardware Experiment Setup

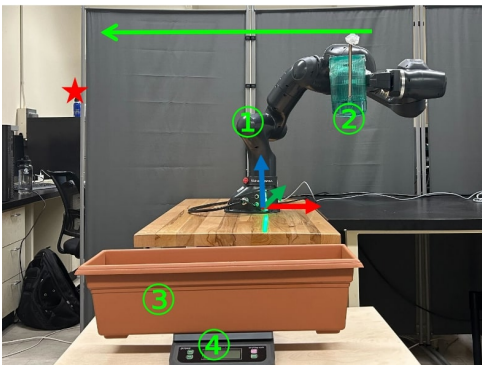


Fig. 16. Mobile water pouring using Franka robot arm. ①: The robot arm. ②: The watering pot. ③: The bar sink. ④: The scale to measure the amount of water poured into the sink. The target is marked as the red star. The long arrow on the top indicates the motion direction, and the RGB coordinate frame is the world frame.

We specifically focus on mobile water pouring by the Franka robot arm. A task setup is shown in Fig. 16. A water pot is gripped by the robot end-effector. The robot needs to move from the starting point $[0.22, -0.5, 0.48]^T$ (with orientation quaternion $[0, -0.707, 0, 0.707]^T$) to target point $[-0.65, -0.5, 0.5]^T$ (with orientation quaternion $[0, -0.707, 0, 0.707]^T$). During the motion, the robot needs to pour more than 50 grams of water into a bar sink. The bar sink is approximately placed in the middle of the robot’s moving path, but the precise size and location of the bar sink are unknown.

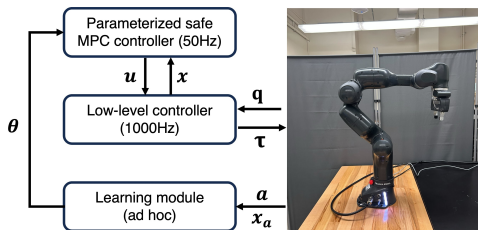


Fig. 17. Components of the hardware Franka arm learning platform

As shown Fig. 17, the hardware Franka arm platform has three main components: the parameterized safe MPC controller (high-level controller), the low-level controller, and a learning module. The high-level safe MPC controller follows the safe MPC formulation of Franka arm reaching game in Section VI-C (recall that the unknown constraint is parameterized by RBFs). The other control parameters of this Safe MPC controller are listed in Table IV. The high-level safe MPC controller receives the end-effector’s current pose x from the low-level controller and solves for the current desired velocity u (defined in (36))

of the end-effector. The low-level controller implements the operation space velocity control to track the desired velocity u given by the high-level controller.

The learning module updates the parameterize θ of the high-level safe MPC controller. The update only happens when the learning module detects a human correction a , which is always accompanied by an end-effector pose x_a where such human correction a is applied to. The learning module implements the proposed safe MPC alignment algorithm.

TABLE IV
PARAMETER LIST IN REAL-WORLD USER STUDY

| Parameter | Value |
|-----------|---------------------------------|
| Q_r | $\text{diag}(0.8, 0.8, 0.8)$ |
| k_q | 0 |
| R_v | $\text{diag}(30, 30, 1)$ |
| R_w | $\text{diag}(0.85, 0.85, 0.85)$ |
| S_r | $\text{diag}(80, 80, 80)$ |
| μ_q | 80 |

In the high-level MPC policy, the cost of the MPC controller is set to penalize the current and target gripper position in Cartesian space, as in Section VI-C. Since it is difficult to explicitly define a parameterized constraint using the state of pouring water, we instead define the constraints of safe water pouring using the robot state. Specifically, we define the same RBF (40) parameterized constraint in Section VI-C, constraining the tilt angle and height of the robot gripper for pouring the water into the sink.

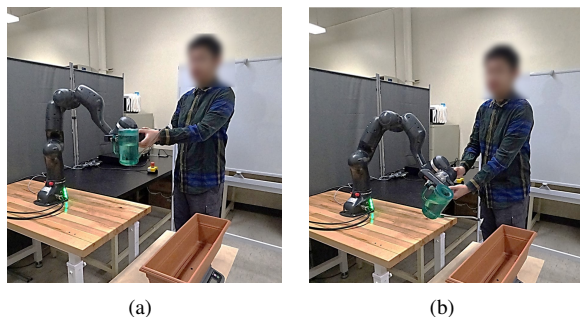


Fig. 18. Illustrations of human correction in the real-world user study. (a) A human user applies force to the robot. (b) The human moves the robot to the desired configuration to pour the water into the bar sink. The delta position of the end effector is used as human directional correction, as in (42).

As shown in Fig. 18, to give a physical correction to the Franka robot arm, a human user can physically touch/hold any link of the robot arm, and the applied force will immediately activate the zero-torque control mode. Suppose the joint positions of the robot arm before and after human physical correction are $\mathbf{q}_{\text{before}}$ and $\mathbf{q}_{\text{after}}$, respectively, we calculate the corresponding raw human correction a_r using

$$\mathbf{a}_r = \mathbf{J}(\mathbf{q}_{\text{before}})(\mathbf{q}_{\text{after}} - \mathbf{q}_{\text{before}}), \quad (42)$$

with \mathbf{J} the Jacobian of the end-effector. The above calculated $\mathbf{a}_r \in \mathbb{R}^6$ is considered as the directional displacement of the end-effector pose, intended by the human user. In the computed $\mathbf{a}_r \in \mathbb{R}^6$, we mask the entries in the other dimensions with 0s and only keep the entries corresponding to the tilt angle

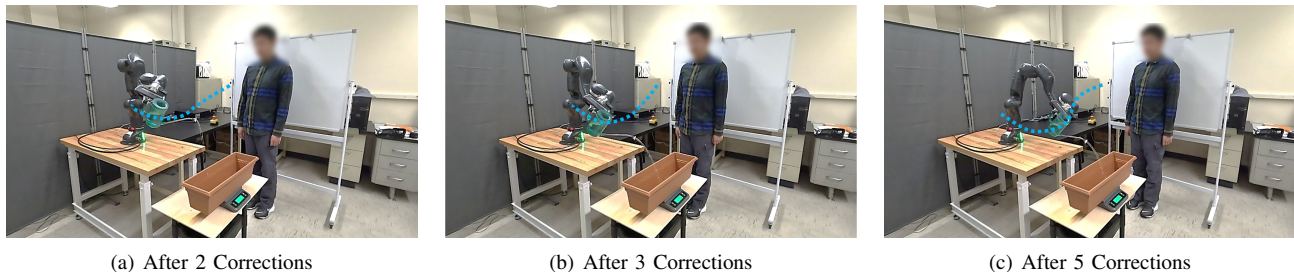


Fig. 19. Illustrations of one trial of the real-world study. The trajectories of the watering pot is denoted by blue dashed lines. (a) After 2 corrections, the arm begins tilting the pot but spills out the water. (b) After 3 corrections, the arm can pour water into the sink but the human is not satisfied with its height and altitude of pouring. (c) After 5 corrections, the arm learns to tilt only along the direction of the x -axis and successfully aligns with human intent.

along x -axis and the height in z -axis, since they are the only dimensions relevant to the given task. The masked vector are is as the actual human correction α fed to the learning module.

B. Participants, Procedures, and Metrics

All participants recruited for the two simulation games in Section VI-D also take part in the hardware experiment user study. They are told of the objective before starting trials. Similar to part VI-C, one episode is defined as one robot motion from the starting gripper position to the target position. One trial means one run of the control with multiple episodes (with a maximum of 15 corrections). During corrections, the nozzle of the water pot is sealed, and we switch to the unsealed nozzle and measure the amount of water poured into the flower pot after the user is satisfied with the motion of the robot motion. The success trial is defined when the amount of poured water is over 50g. Each user performs 5 trials, and the same metrics in Section VI-D are recorded.

C. Result and Analysis

In real-world robot experiments, the success rate is $84.0\% \pm 16.7\%$ and the average number of corrections in successful trials is 6.88 ± 3.26 . The results show the efficacy and efficiency of the proposed method in real-world robot learning applications. To illustrate the robot learning progress, in Fig. 19, we use one trial of the user study to show the robot behavior at different numbers of human corrections.

Since the task of this real-world Franka arm experiment is similar to the simulated Franka arm reaching game in Section VI-C, we compare the user study results for both and have the following conclusion and analysis.

(I) *The real-world experiment has a slightly lower success rate:* While the difference between simulations and real-world experiments is small in success rate, we have identified some factors during our experiment that may contribute to such lower success rate, which includes both the human factors and hardware factors. On human factors, most of the participants have no experience or knowledge in operating robot hardware, and thus when directly interacting with hardware, their corrections can be conservative or ineffective due to safety considerations. On the hardware side, some error sources, such as noisy correction signals, and the possible timing lag between the recorded correction-happening robot state and the

human intended correction-happening state, can contribute to the failure of the learning.

(II) *The real-world experiment has a less number of human corrections:* This could be attributed to two reasons. First, the constraint needed for accomplishing the water pouring task in the real-world experiment could be more relaxed than the constraint for accomplishing the narrow slot passing task in the simulation game in Section VI-C. This makes the safety constraints easy to learn for the real-world task. Second, different from simulation games, where human users can only perceive the motion of the robot arm from the screen, a human user has a better perception of the robot’s motion in a real-world experiment. A good perception of the robot’s motion could help humans give more effective feedback each time, reducing the total number of human interactions for successful robot learning.

D. Discussion

Based on the observations in both the hardware and simulation user studies, we discuss some design choices and potential limitations of the proposed *safe MPC alignment* algorithm.

1) *Learning Task-Independent Safety Constraints:* In the real-world and simulation experiments, due to the insufficiency of task sampling, the learned safety constraint can be task-dependent, instead of task-independent. For instance, in the drone navigation game in Section VI-B, since the three task targets are placed above the gate, the learned constraint shown in Fig. 15 can only reflect the upper edge of the gate constraints. One limitation of this is that the learned task constraints have poor generalization to new tasks, which are far from previously encountered. For example, in drone navigation, if a new target is placed below the gate, the drone with the learned safety constraint Fig. 15 will fail.

To improve the generalization of the learned safety constraints or learning task-independent safety constraints, one solution is to increase the diversity of task samples. By doing so, it is expected that the robot can receive human correction on the entire boundary of the safety region, making the learned safety constraints task irrelevant.

2) *Robustness Against Human Irrationality:* Our proposed *safe MPC alignment* method is based on the cutting hypothesis. In our formulation, we define a hypothesis cut (7) based on an average of multiple human corrections, such an averaging treatment is to mitigate human mistakes for one cut. But still,

in practice, human irrationality can lead to the wrong cut of the hypothesis space, which constitutes the main reason for failure in user studies. For example, in the drone navigation game, we found that failure game trials usually happen when a human gives too many wrong directional corrections at the beginning of the trial. A failure case is shown in Fig. 20.



Fig. 20. One illustration of the failure case in the drone user study. A human user makes a false "up" correction at the beginning and fails to correct the motion of the drone.

To further improve the robustness of the method against human mistakes, two extensions of the current method can be used on top of our proposed algorithm. The first is to add a relaxation factor $\epsilon \geq 0$ in our cutting hypothesis. For example, we can re-write (7) as

$$\forall \theta_H \in \bar{\Theta}_H, \mathbb{E}_a \langle \mathbf{a}, -\nabla B(\xi_\theta^\gamma, \theta_H) \rangle + \epsilon \geq 0. \quad (43)$$

Another extension is to add a selection mechanism on human correction. For example, one can use some statistical method to distinguish and rule out mistake corrections before performing a hypothesis cut. We will leave those possible extensions in our future work.

VIII. CONCLUSION

This paper proposes safe MPC alignment method to online learn a safety constraint in robot safe MPC controllers from human directional feedback. The method, named hypothesis space cutting, has geometric interpretation: it exponentially cuts the hypothesis space based on each received human directional feedback. The method has a provable guarantee for the upper bound of the total number of human feedback, and also can declare hypothesis misspecification. A numeric example, two user studies on simulation games, and a user study on the real-world robot arm, covering varying robot tasks, were used to validate the effectiveness and efficiency of the proposed approach. The results show that the proposed method can learn safety constraints effectively and efficiently. To our knowledge, this is the first certifiable method to enable online learning of safety constraints with human feedback.

REFERENCES

- [1] Kim P Wabersich, Andrew J Taylor, Jason J Choi, Koushil Sreenath, Claire J Tomlin, Aaron D Ames, and Melanie N Zeilinger. Data-driven safety filters: Hamilton-jacobi reachability, control barrier functions, and predictive methods for uncertain systems. *IEEE Control Systems Magazine*, 43(5):137–177, 2023.
- [2] Shangding Gu, Long Yang, Yali Du, Guang Chen, Florian Walter, Jun Wang, Yaodong Yang, and Alois Knoll. A review of safe reinforcement learning: Methods, theory and applications. *arXiv preprint arXiv:2205.10330*, 2022.

- [3] Glen Chou, Dmitry Berenson, and Necmiye Ozay. Learning constraints from demonstrations. In *Algorithmic Foundations of Robotics XIII: Proceedings of the 13th Workshop on the Algorithmic Foundations of Robotics 13*, pages 228–245. Springer, 2020.
- [4] David Lindner, Xin Chen, Sebastian Tschiatschek, Katja Hofmann, and Andreas Krause. Learning safety constraints from demonstrations with unknown rewards. *arXiv preprint arXiv:2305.16147*, 2023.
- [5] Dexter RR Scobee and S Shankar Sastry. Maximum likelihood constraint inference for inverse reinforcement learning. *arXiv preprint arXiv:1909.05477*, 2019.
- [6] Dylan P Losey, Andrea Bajcsy, Marcia K O'Malley, and Anca D Dragan. Physical interaction as communication: Learning robot objectives online from human corrections. *The International Journal of Robotics Research*, 41(1):20–44, 2022.
- [7] Wanxin Jin, Todd D Murphey, Zehui Lu, and Shaoshuai Mou. Learning from human directional corrections. *IEEE Transactions on Robotics*, 39(1):625–644, 2022.
- [8] Rudolf Emil Kalman. When is a linear control system optimal? 1964.
- [9] Andrew Y Ng, Stuart Russell, et al. Algorithms for inverse reinforcement learning. In *icml*, volume 1, page 2, 2000.
- [10] Pieter Abbeel and Andrew Y Ng. Apprenticeship learning via inverse reinforcement learning. In *Proceedings of the twenty-first international conference on Machine learning*, page 1, 2004.
- [11] Nathan D Ratliff, J Andrew Bagnell, and Martin A Zinkevich. Maximum margin planning. In *Proceedings of the 23rd international conference on Machine learning*, pages 729–736, 2006.
- [12] Brian D Ziebart, Andrew L Maas, J Andrew Bagnell, Anind K Dey, et al. Maximum entropy inverse reinforcement learning. In *Aaai*, volume 8, pages 1433–1438. Chicago, IL, USA, 2008.
- [13] Katja Mombaur, Anh Truong, and Jean-Paul Laumond. From human to humanoid locomotion—an inverse optimal control approach. *Autonomous robots*, 28:369–383, 2010.
- [14] Peter Englert, Ngo Anh Vien, and Marc Toussaint. Inverse kkt: Learning cost functions of manipulation tasks from demonstrations. *The International Journal of Robotics Research*, 36(13-14):1474–1488, 2017.
- [15] Harish Ravichandar, Athanasios S Polydoros, Sonia Chernova, and Aude Billard. Recent advances in robot learning from demonstration. *Annual review of control, robotics, and autonomous systems*, 3:297–330, 2020.
- [16] Ashesh Jain, Shikhar Sharma, Thorsten Joachims, and Ashutosh Saxena. Learning preferences for manipulation tasks from online coactive feedback. *The International Journal of Robotics Research*, 34(10):1296–1313, 2015.
- [17] Paul F Christiano, Jan Leike, Tom Brown, Miljan Martic, Shane Legg, and Dario Amodei. Deep reinforcement learning from human preferences. *Advances in neural information processing systems*, 30, 2017.
- [18] Dorsa Sadigh, Anca D. Dragan, S. Shankar Sastry, and Sanjit A. Seshia. Active preference-based learning of reward functions. In *Robotics: Science and Systems*, 2017.
- [19] Borja Ibarz, Jan Leike, Tobias Pohlen, Geoffrey Irving, Shane Legg, and Dario Amodei. Reward learning from human preferences and demonstrations in atari. *Advances in neural information processing systems*, 31, 2018.
- [20] Kimin Lee, Laura M Smith, and Pieter Abbeel. Pebble: Feedback-efficient interactive reinforcement learning via relabeling experience and unsupervised pre-training. In Marina Meila and Tong Zhang, editors, *Proceedings of the 38th International Conference on Machine Learning*, volume 139 of *Proceedings of Machine Learning Research*, pages 6152–6163. PMLR, 18–24 Jul 2021.
- [21] Donald Joseph Hejna III and Dorsa Sadigh. Few-shot preference learning for human-in-the-loop rl. In *Conference on Robot Learning*, pages 2014–2025. PMLR, 2023.
- [22] Vivek Myers, Erdem Biyik, and Dorsa Sadigh. Active reward learning from online preferences. In *2023 IEEE International Conference on Robotics and Automation (ICRA)*, pages 7511–7518, 2023.
- [23] Vivek Myers, Erdem Biyik, Nima Anari, and Dorsa Sadigh. Learning multimodal rewards from rankings. In Aleksandra Faust, David Hsu, and Gerhard Neumann, editors, *Proceedings of the 5th Conference on Robot Learning*, volume 164 of *Proceedings of Machine Learning Research*, pages 342–352. PMLR, 08–11 Nov 2022.
- [24] Ralph Allan Bradley and Milton E Terry. Rank analysis of incomplete block designs: I. the method of paired comparisons. *Biometrika*, 39(3/4):324–345, 1952.
- [25] Joey Hejna, Rafael Rafailov, Harshit Sikchi, Chelsea Finn, Scott Niekum, W Bradley Knox, and Dorsa Sadigh. Contrastive preference learning: Learning from human feedback without rl. *arXiv preprint arXiv:2310.13639*, 2023.

- [26] Siddharth Karamcheti, Raj Pallei, Yuchen Cui, Percy Liang, and Dorsa Sadigh. Shared autonomy for robotic manipulation with language corrections. In *ACL Workshop on Learning with Natural Language Supervision*, 2022.
- [27] Yuchen Cui, Siddharth Karamcheti, Raj Pallei, Nidhya Shivakumar, Percy Liang, and Dorsa Sadigh. No, to the right: Online language corrections for robotic manipulation via shared autonomy. In *Proceedings of the 2023 ACM/IEEE International Conference on Human-Robot Interaction*, pages 93–101, 2023.
- [28] Megha Srivastava, Noah Goodman, and Dorsa Sadigh. Generating language corrections for teaching physical control tasks. In *International Conference on Machine Learning*, pages 32561–32574. PMLR, 2023.
- [29] Lihan Zha, Yuchen Cui, Li-Heng Lin, Minae Kwon, Montserrat G. Arenas, Andy Zeng, Fei Xia, and Dorsa Sadigh. Distilling and retrieving generalizable knowledge for robot manipulation via language corrections. In *International Conference on Robotics and Automation (ICRA)*, may 2024.
- [30] Lucy Xiaoyang Shi, Zheyuan Hu, Tony Z Zhao, Archit Sharma, Karl Pertsch, Jianlan Luo, Sergey Levine, and Chelsea Finn. Yell at your robot: Improving on-the-fly from language corrections. *arXiv preprint arXiv:2403.12910*, 2024.
- [31] Andrea Bajcsy, Dylan P Losey, Marcia K O’Malley, and Anca D Dragan. Learning robot objectives from physical human interaction. In *Conference on robot learning*, pages 217–226. PMLR, 2017.
- [32] Andrea Bajcsy, Dylan P Losey, Marcia K O’Malley, and Anca D Dragan. Learning from physical human corrections, one feature at a time. In *Proceedings of the 2018 ACM/IEEE International Conference on Human-Robot Interaction*, pages 141–149, 2018.
- [33] Dylan P Losey and Marcia K O’Malley. Including uncertainty when learning from human corrections. In *Conference on Robot Learning*, pages 123–132. PMLR, 2018.
- [34] Jason Y Zhang and Anca D Dragan. Learning from extrapolated corrections. In *2019 International Conference on Robotics and Automation (ICRA)*, pages 7034–7040. IEEE, 2019.
- [35] Mengxi Li, Alper Canberk, Dylan P Losey, and Dorsa Sadigh. Learning human objectives from sequences of physical corrections. In *2021 IEEE International Conference on Robotics and Automation (ICRA)*, pages 2877–2883. IEEE, 2021.
- [36] Shaanak A Mehta and Dylan P Losey. Unified learning from demonstrations, corrections, and preferences during physical human-robot interaction. *ACM Transactions on Human-Robot Interaction*, 2023.
- [37] Kimin Lee, Laura Smith, and Pieter Abbeel. Pebble: Feedback-efficient interactive reinforcement learning via relabeling experience and unsupervised pre-training. *arXiv preprint arXiv:2106.05091*, 2021.
- [38] Glen Chou, Necmiye Ozay, and Dmitry Berenson. Learning parametric constraints in high dimensions from demonstrations. In *Conference on Robot Learning*, pages 1211–1230. PMLR, 2020.
- [39] Ashish Gaurav, Kasra Rezaee, Guliang Liu, and Pascal Poupart. Learning soft constraints from constrained expert demonstrations. In *The Eleventh International Conference on Learning Representations*, 2023.
- [40] Konwoo Kim, Gokul Swamy, Zuxin Liu, Ding Zhao, Sanjiban Choudhury, and Steven Z Wu. Learning shared safety constraints from multi-task demonstrations. *Advances in Neural Information Processing Systems*, 36, 2024.
- [41] Glen Chou, Necmiye Ozay, and Dmitry Berenson. Learning constraints from locally-optimal demonstrations under cost function uncertainty. *IEEE Robotics and Automation Letters*, 5(2):3682–3690, 2020.
- [42] Glen Chou, Dmitry Berenson, and Necmiye Ozay. Uncertainty-aware constraint learning for adaptive safe motion planning from demonstrations. In *Conference on Robot Learning*, pages 1612–1639. PMLR, 2021.
- [43] Glen Chou, Hao Wang, and Dmitry Berenson. Gaussian process constraint learning for scalable chance-constrained motion planning from demonstrations. *IEEE Robotics and Automation Letters*, 7(2):3827–3834, 2022.
- [44] Kaylene C Stocking, D Livingston McPherson, Robert P Matthew, and Claire J Tomlin. Maximum likelihood constraint inference on continuous state spaces. In *2022 International Conference on Robotics and Automation (ICRA)*, pages 8598–8604. IEEE, 2022.
- [45] Shehryar Malik, Usman Anwar, Alireza Aghasi, and Ali Ahmed. Inverse constrained reinforcement learning. In *International conference on machine learning*, pages 7390–7399. PMLR, 2021.
- [46] David L McPherson, Kaylene C Stocking, and S Shankar Sastry. Maximum likelihood constraint inference from stochastic demonstrations. In *2021 IEEE Conference on Control Technology and Applications (CCTA)*, pages 1208–1213. IEEE, 2021.
- [47] Mattijs Baert, Pietro Mazzaglia, Sam Leroux, and Pieter Simoens. Maximum causal entropy inverse constrained reinforcement learning. *arXiv preprint arXiv:2305.02857*, 2023.
- [48] Daehyung Park, Michael Noseworthy, Rohan Paul, Subhro Roy, and Nicholas Roy. Inferring task goals and constraints using bayesian nonparametric inverse reinforcement learning. In *Conference on robot learning*, pages 1005–1014. PMLR, 2020.
- [49] Dimitris Papadimitriou, Usman Anwar, and Daniel S Brown. Bayesian methods for constraint inference in reinforcement learning. *Transactions on Machine Learning Research*, 2022.
- [50] Wanxin Jin, Shaoshuai Mou, and George J Pappas. Safe ponytraygin differentiable programming. *Advances in Neural Information Processing Systems*, 34:16034–16050, 2021.
- [51] Russ Tedrake. Underactuated robotics: Learning, planning, and control for efficient and agile machines course notes for mit 6.832. *Working draft edition*, 3(4):2, 2009.
- [52] Ruohan Zhang, Dhruva Bansal, Yilun Hao, Ayano Hiranaka, Jialu Gao, Chen Wang, Roberto Martín-Martín, Li Fei-Fei, and Jiajun Wu. A dual representation framework for robot learning with human guidance. In *Conference on Robot Learning*, pages 738–750. PMLR, 2023.
- [53] Erdem Bıyık, Aditi Talati, and Dorsa Sadigh. Aprel: A library for active preference-based reward learning algorithms. In *2022 17th ACM/IEEE International Conference on Human-Robot Interaction (HRI)*, pages 613–617. IEEE, 2022.
- [54] Andreea Bobu, Andrea Bajcsy, Jaime F Fisac, Sampada Deglurkar, and Anca D Dragan. Quantifying hypothesis space misspecification in learning from human-robot demonstrations and physical corrections. *IEEE Transactions on Robotics*, 36(3):835–854, 2020.
- [55] Stephen Casper, Xander Davies, Claudia Shi, Thomas Krendl Gilbert, Jérémy Scheurer, Javier Rando, Rachel Freedman, Tomasz Korbak, David Lindner, Pedro Freire, et al. Open problems and fundamental limitations of reinforcement learning from human feedback. *arXiv preprint arXiv:2307.15217*, 2023.
- [56] Luis A Rademacher. Approximating the centroid is hard. In *Proceedings of the twenty-third annual symposium on Computational geometry*, pages 302–305, 2007.
- [57] Aditi Laddha and Santosh S Vempala. Convergence of gibbs sampling: coordinate hit-and-run mixes fast. *Discrete & Computational Geometry*, pages 1–20, 2023.
- [58] Simon Tong and Daphne Koller. Support vector machine active learning with applications to text classification. *Journal of machine learning research*, 2(Nov):45–66, 2001.
- [59] Stephen P Boyd and Lieven Vandenberghe. *Convex optimization*. Cambridge university press, 2004.
- [60] Gaurav R Ghosal, Matthew Zurek, Daniel S Brown, and Anca D Dragan. The effect of modeling human rationality level on learning rewards from multiple feedback types. In *Proceedings of the AAAI Conference on Artificial Intelligence*, volume 37, pages 5983–5992, 2023.
- [61] Emanuel Todorov, Tom Erez, and Yuval Tassa. Mujoco: A physics engine for model-based control. In *2012 IEEE/RSJ International Conference on Intelligent Robots and Systems*, pages 5026–5033. IEEE, 2012.
- [62] Sergei Pavlovich Tarasov. The method of inscribed ellipsoids. In *Soviet Mathematics-Doklady*, volume 37, pages 226–230, 1988.

APPENDIX A

PROOF OF LEMMAS AND THEOREMS

A. Proof of Lemma 2

Proof. We prove this lemma by induction. First, we have $\bar{\Theta}_H \subset \Theta_0$. Suppose $\bar{\Theta}_H \subset \Theta_{i-1}$, $i = 1, 2, 3, \dots$. Due to the condition $\bar{\Theta}_H \subset \mathcal{C}_i$ in (12), following the update (13), we have $\bar{\Theta}_H \subset \Theta_i = \Theta_{i-1} \cap \mathcal{C}_i$, which completes the proof. \square

B. Proof of Lemma 4

Proof. For any $i = 1, 2, 3, \dots$, the plan $\xi_{\theta_i}^\gamma = \{u_{0:T-1}^{\theta_i, \gamma}, x_{0:T}^{\theta_i, \gamma}\}$ is a solution to the optimization (3), with $\theta = \theta_i$. Recall Lemma 1, $g_{\theta_i}(\xi_{\theta_i}^\gamma) < 0$. Extending the feature-weight expression of $g_{\theta_i}(\xi_{\theta_i}^\gamma)$, one can get $\theta_i^\top \phi(\xi_{\theta_i}^\gamma) < -\phi_0(\xi_{\theta_i}^\gamma)$. Since the optimal solution $u_{0:T-1}^{\theta_i, \gamma}$ is a minimizer to (3), it means

$$\nabla B(\xi_{\theta_i}^\gamma, \theta_i) = 0. \quad (44)$$

Note that with $g_{\theta_i}(\xi_{\theta_i}^\gamma) < 0$, the above $\nabla B(\xi_{\theta_i}^\gamma, \theta_i)$ is well defined. With (44),

$$\langle \mathbf{a}, \nabla B(\xi_{\theta_i}^\gamma, \theta_i) \rangle = 0, \quad (45)$$

always holds. Extending the above (45) leads to

$$\langle \mathbf{a}, \nabla J(\xi_{\theta_i}^\gamma) \rangle - \gamma \frac{1}{g_{\theta_i}(\xi_{\theta_i}^\gamma)} \langle \mathbf{a}, \nabla g_{\theta_i}(\xi_{\theta_i}^\gamma) \rangle = 0. \quad (46)$$

Due to $-g_{\theta_i}(\xi_{\theta_i}^\gamma) > 0$, one can multiple $-g_{\theta_i}(\xi_{\theta_i}^\gamma)$ on both sides of the above equality, which leads to $\theta_i^\top \mathbf{h}_i = b_i$ based on the definition (16). The second term in (19) directly follows $g_{\theta_i}(\xi_{\theta_i}^\gamma) < 0$. This concludes the proof. \square

C. Proof of Lemma 5

Proof. By Lemma 4, the MVE center $\theta_i = \bar{\mathbf{d}}_{i-1}$ is on the cutting hyperplane $\theta^\top \mathbf{h}_i = b_i$. Directly from [62], one has

$$\frac{\text{Vol}(\Theta_{i-1} \cap \{\theta | \theta^\top \mathbf{h}_i \leq b_i\})}{\text{Vol}(\Theta_{i-1})} \leq 1 - \frac{1}{r}. \quad (47)$$

Since

$$\text{Vol}(\Theta_{i-1} \cap \{\theta | \theta^\top \mathbf{h}_i \leq b_i\}) \geq \text{Vol}(\Theta_{i-1} \cap \mathcal{C}_i) = \text{Vol}(\Theta_i), \quad (48)$$

based on (12), (13), one can get

$$\frac{\text{Vol}(\Theta_i)}{\text{Vol}(\Theta_{i-1})} \leq 1 - \frac{1}{r}. \quad (49)$$

Which concludes the proof. \square

D. Proof of Theorem 1

Proof. We complete the proof in two parts. First, we prove the number of learning iterations is less than K , then we use this to prove there will be a $\theta_k \in \bar{\Theta}_H$, $k = 0, 1, 2, \dots, K-1$.

We first prove the total number of iterations must be less than K by contradiction. Suppose the learning iteration number $i \geq K$. With recursively applying lemma 5, one can obtain

$$\text{Vol}(\Theta_i) \leq (1 - \frac{1}{r})^i \text{Vol}(\Theta_0). \quad (50)$$

When $i \geq K$,

$$\text{Vol}(\Theta_i) < \frac{\tau_r \rho_H^r}{\text{Vol}(\Theta_0)} \text{Vol}(\Theta_0) = \tau_r \rho_H^r \leq \text{Vol}(\bar{\Theta}_H) \quad (51)$$

However, from Lemma 2, one has $\bar{\Theta}_H \subset \Theta_i$, meaning $\text{Vol}(\bar{\Theta}_H) \leq \text{Vol}(\Theta_i)$. This leads to a contradiction with (51). Therefore, the total number of iterations must be less than K .

Next, we prove $\exists k < K$ such that $\theta_k \in \bar{\Theta}_H$. In contradiction, suppose $\forall k < K$, $\theta_k \notin \bar{\Theta}_H$. By Lemma 2, this means that for all $i < K$, $\bar{\Theta}_H \subset \mathcal{C}_i$. Then, the algorithm will continue for $i = K$. Consequently, the total number of iterations can reach K , which contradicts that the algorithm will terminate within K iterations. This concludes the proof. \square

E. Proof of Theorem 2

Proof. We complete the proof in two parts. First we prove the algorithm converges to Θ^* which has $\text{Vol}(\Theta^*) = 0$. Based on this, we next prove $\Theta^* \cap \text{int } \Theta_0 = \emptyset$.

We first prove the algorithm converges to Θ^* which has $\text{Vol}(\Theta^*) = 0$. Given the condition $\Theta_0 \cap \bar{\Theta}_H = \emptyset$, the algorithm will never terminate because $\forall i = 1, 2, 3, \dots, \infty$, $\mathcal{C}_i \supset \bar{\Theta}_H$ due to Lemma 2. Since the volume of the initial hypothesis space is finite, by applying Lemma 5 we have

$$\text{Vol}(\Theta^*) = \lim_{i \rightarrow \infty} (1 - \frac{1}{r})^i \text{Vol}(\Theta_0) = 0. \quad (52)$$

Next, we prove $\Theta^* \cap \text{int } \Theta_0 = \emptyset$ by contradiction. Suppose there exists $\theta \in \Theta^* \cap \text{int } \Theta_0$. Define the ball contained in $\bar{\Theta}_H$ to be $\mathcal{B}(\theta_H^c, \rho_H) = \{\theta \mid \|\theta - \theta_H^c\| \leq \rho_H\} \subseteq \bar{\Theta}_H$ with θ_H^c as the center. By the equation (13), we can note

$$\Theta^* = \Theta_0 \cap \mathcal{C}, \quad (53)$$

with $\mathcal{C} = \bigcap_{i=1}^{\infty} \mathcal{C}_i$ a convex set. So we have

$$\Theta^* \subseteq \mathcal{C}. \quad (54)$$

By equation (12),

$$\mathcal{B}_H \subseteq \bar{\Theta}_H \subseteq \mathcal{C}. \quad (55)$$

From the relationship between sets above, $\theta_H^c \in \mathcal{C}$, $\hat{\theta} \in \mathcal{C}$.

Since $\theta_H^c \notin \Theta_0$, there exists $\mu > 0$ such that

$$\tilde{\theta} = \hat{\theta} + \mu(\theta_H^c - \hat{\theta}) \in \text{int } \Theta_0. \quad (56)$$

Then, one can define a ball $\mathcal{B}(\tilde{\theta}, d)$ centered at $\tilde{\theta}$ with radius

$$d = \min_{\theta \in \text{bd } \Theta_0} \|\tilde{\theta} - \theta\|. \quad (57)$$

Thus, $\mathcal{B}(\tilde{\theta}, d) \subset \text{int } \Theta_0$.

Next, we will show $\mathcal{B}(\tilde{\theta}, \mu\rho_H) \subset \mathcal{C}$. In fact, for any θ satisfying $\|\theta - \tilde{\theta}\| \leq \mu\rho_H$, one has

$$\begin{aligned} \theta &= \mu \left(\frac{1}{\mu} (\theta - \tilde{\theta}) + \theta_H^c \right) + \tilde{\theta} - \mu \theta_H^c \\ &= \underbrace{\mu \left(\frac{1}{\mu} (\theta - \tilde{\theta}) + \theta_H^c \right)}_{\in \mathcal{B}_H \subseteq \mathcal{C}} + (1 - \mu) \underbrace{\tilde{\theta}}_{\in \Theta^* \subseteq \mathcal{C}}. \end{aligned} \quad (58)$$

The convexity of \mathcal{C} leads to $\theta \in \mathcal{C}$, which means the ball $\mathcal{B}_\mu \triangleq \{\theta \mid \|\tilde{\theta} - \theta\| \leq \mu\rho_H\} \subset \mathcal{C}$.

Let a new ball be $\mathcal{B}(\tilde{\theta}, \min(\mu\rho_H, d))$. Based on the previous two results of $\mathcal{B}(\tilde{\theta}, d) \subset \text{int } \Theta_0$ and $\mathcal{B}(\tilde{\theta}, \mu\rho_H) \subset \mathcal{C}$, one has $\mathcal{B}(\tilde{\theta}, \min(\mu\rho_H, d)) \subset (\Theta_0 \cap \mathcal{C}) = \Theta^*$. As a result,

$$\text{Vol}(\Theta^*) \geq \text{Vol } \mathcal{B}(\tilde{\theta}, \min(\mu\rho_H, d)) > 0 \quad (59)$$

which contradicts $\text{Vol}(\Theta^*) = 0$ from (52). Thus, $\Theta^* \cap \text{int } \Theta_0 = \emptyset$ must hold. This completes the proof. \square